

HEPA Filter Failure Modes at Elevated Pressure, Temperature and Moisture

by

Werner Bergman and Gerard Garcia¹

Aerosol Science, LLC, Stanwood, WA, wbergman@aerosolscience.com

¹Consultant, gerardgarcia.me@gmail.com

Abstract

This report presents an analysis of HEPA filter failure modes at elevated pressure, temperature, and moisture using published experimental studies. The test results presented by Giffin et al (2012) and Waggoner (2012a) on filter pleat collapse are analyzed in terms of probability of HEPA filter failure as a function of differential pressure at various temperatures and relative humidity for several different filter designs. Pleat collapse occurs for separatorless HEPA filters above 8 in. WC under ambient temperature and dry conditions and above 6 inches at moderately high temperatures (130°F). A theory for pleat collapse based on studies of mechanical plate deflection is presented and is used in the analysis.

This report also reviews the HEPA filter failures at higher differential pressures due to the bending of the HEPA filter pack and due to the rupture of pleat ends. A statistical analysis of these filter failures is performed for both wet and dry conditions.

Pleat Collapse

Pleat collapse, illustrated in Figure 1, is the undesirable feature of a pleated filter in which the individual pleats collapse due to the applied pressure of moving air. The use of rigid separators like corrugated aluminum separators prevent pleat collapse. Separatorless HEPA filters that use embossments of the filter medium prevent pleat collapse under mild conditions of temperature and pressure drop.

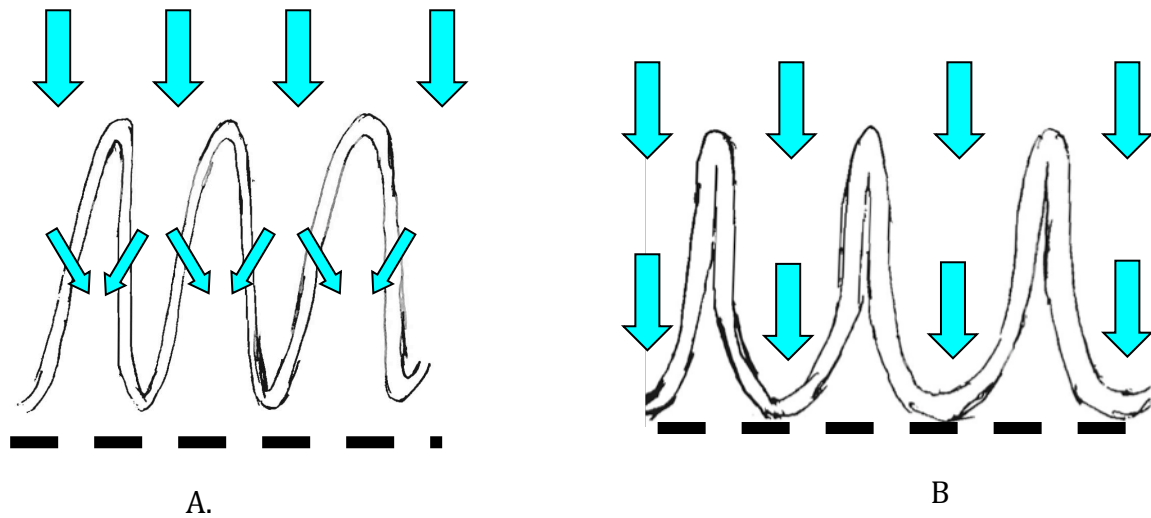


Figure 1. Cross section drawing of a portion of a pleated filter pack for (A) a filter with no pleat collapse, and the pack maintains a distance from the filter screen and (B) a filter with pleat collapse, and the filter pack is compressed against the filter screen.

Pleat collapse occurs when the filter medium has insufficient stiffness to maintain the desired shape and is deflected onto the adjoining medium of the pleat if there are no separators or if the separators are not effective. The medium stiffness can be significantly reduced at higher temperatures and when the medium becomes wet. For filters that use embossments of the medium to form dimples or ridges as separators, the strength of these separators decreases with increasing temperature and when the medium becomes wet. As the pleats begin to collapse, the reduced filter medium area results in a higher pressure drop, which in turn causes even greater pleat collapse. Once the pleats begin to collapse, the unstable feed-forward process results in a rapid increase in pressure drop and can lead to medium tears if the fan has sufficient power.

Particle loading contributes to pleat collapse by increasing the filter pressure drop as illustrated in Figure 2. However, since the particle deposits do not interact with the fiber bonds that are responsible for the filter medium stiffness, the deposits do not alter the stiffness of the medium. The particle deposits only increase the pressure drop across the filter in a similar fashion as increased air flow.

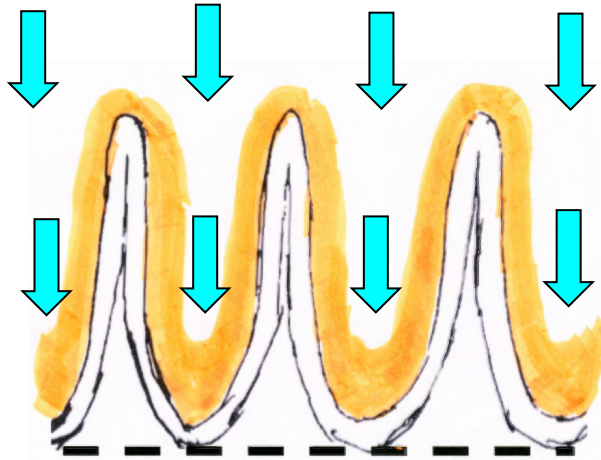


Figure 2. Cross section of filter pleats loaded with particles that increase the pressure drop across the pleats at a constant velocity. The particle deposits do not alter the stiffness of the filter medium.

Pleat Collapse with Radial Flow HEPA Filters

The experimental measurements on Flanders radial flow HEPA filters conducted at the Institute for Clean Energy Technology (ICET) at Mississippi State University (MSU) were used to analyze pleat collapse in this report (Giffin et al, 2012; Waggoner, 2012a, 2012b). Flanders radial flow HEPA filters, shown in Figure 3 were used in the MSU tests. Two models of these filters were tested: a safe-change (SC) and a remote-change (RC) model that differed slightly for used in two different filter housings.

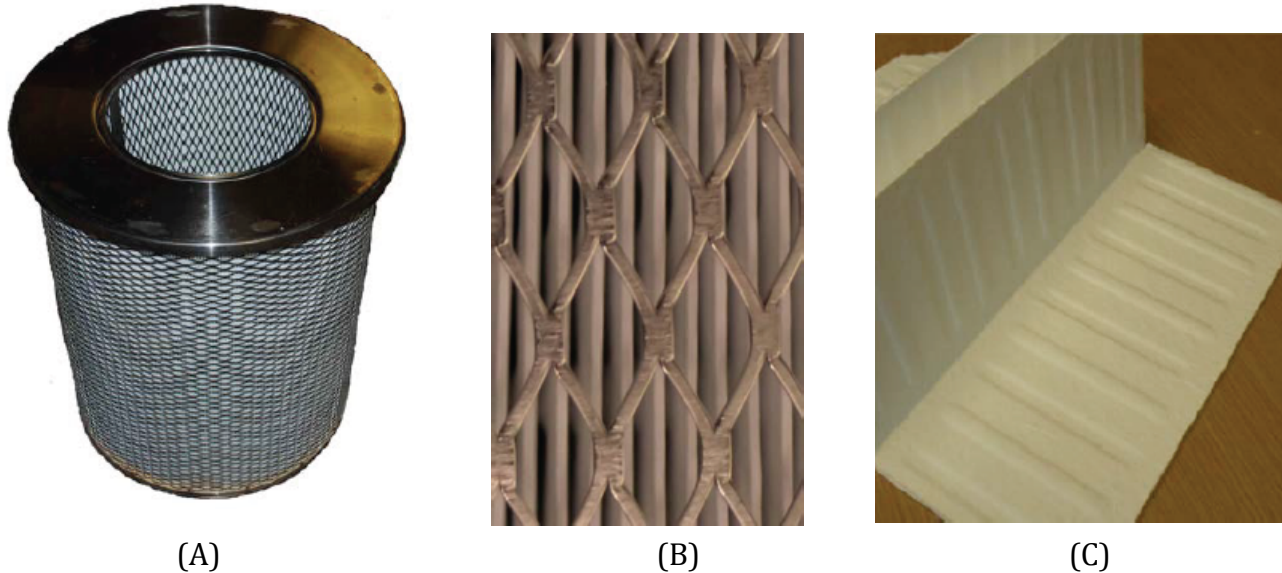


Figure 3. Flanders (A) 2,000 cfm remote change filter, (B) close-up of outside pleats and (C) cut out portion of filter pack showing the 3” deep pleat with embossed dimples (Giffin et al, 2012).

Table 1. Estimated filter parameters for Flanders Radial Flow HEPA filter used in this study

Dimension	WTP Radial Filter Type		Units
	Remote	Safe Change	
Filter Inlet Opening ID	11.0	13.0	in.
Filter Pack OD	18.5	19.8	in.
Filter Pack ID	12.5	13.8	in.
Pack Medium Width	23	23	in.
Estimated Medium Thickness	0.018	0.018	in.
Minimum Effective Filter Media Area	308	308	sq. ft.
Pleat depth	3.00	3.00	in.
Estimated Number of Pleats	321	323	
Pleats Per Inch @ Filter Inlet Face	8.18	7.47	ppi
Pleats Per inch @ Filter outlet face	5.52	5.20	ppi
Average ppi for filter	6.85	6.34	ppi

The initial pressure drops of the Flanders SC and RC filters at 2000 cfm measured at the DOE Filter Test Facility (FTF), Flanders, and MSU is given in Table 2 (Paxton et al, 2012;Waggoner, 2012b). The FTF and Flanders data agree closely, and the MSU data is about 0.1 in. WC lower. These differences between the different facilities are likely due to the different orifice diameters used in the filter test housings, but that information was not available.

The higher pressure drop of the RC filters (MSU average 1.39 in. WC) compared to the SC filters (MSU average 0.93 in. WC) is due to a more compressed filter pack and a more restrictive inlet opening for the RC filter as seen in Table 1. Since the same orifice opening of 13 inches in the MSU filter housing was used for both SC and RC filters, the ΔP due to the filter inlet opening could be subtracted for the SC filter, but not for the RC filter. The housing orifice opening would have to be 11 in. diameter to remove the ΔP due to the RC inlet. Computing the equivalent tare for the 11 in. diameter orifice by assuming a constant discharge coefficient as the 13 in. diameter orifice yields an unrealistic pressure drop and was therefore not used here. Thus the ΔP values for the RC filters in this report includes the additional resistance of the 11 in. grab ring used for remote handling. This additional resistance introduces a non-linearity in the ΔP versus flow curve for the RC filter and a small error in parameters derived from the RC ΔP values. Since the corrected ΔP for the RC filter must be greater than the ΔP for the SC filter, the correction must be less than 0.46 in. WC at 2000 cfm. Generating a tare ΔP curve for an 11 in. orifice in the MSU housing could be applied in future studies to eliminate the grab ring contribution to the RC filter ΔP .

Table 2. Pressure drop of new Flanders SC and RC HEPA filters tested at the DOE Filter Test Facility (FTF), Flanders and at MSU at 2,000 cfm.

	ΔP , in. WC				ΔP , in. WC		
Safe Change ID	DOE FTF	Flanders	MSU	Remote Change ID	DOE FTF	Flanders	MSU
SC-001	1.08	1.01	0.9	RC-001	1.67	1.45	1.4
SC-002	0.96	1.01	0.9	RC-002	1.38	1.45	1.34
SC-003	1.08	1.08	1.0	RC-003	1.54	1.49	1.4
SC-004	1.12	--	0.9*	RC-004	1.2	1.41	1.4
Average=	1.06	1.03	0.93	RC-007	1.73	1.52	1.4
				RC-008	1.48	1.46	1.34
				RC-009	1.50	1.51	1.4
				RC-010	1.3	--	1.4
				Average=	1.48	1.47	1.39

*From graphs

Ambient Temperature and Humidity Tests

The MSU tests consisted of loading the radial flow HEPA filters with test aerosols of $Al(OH)_3$ powder, carbon black, or Arizona Road Dust at a constant 2,000 cfm at ambient temperature and relative humidity (Giffin et al, 2012). The pressure drop across the filter would be monitored during the particle loading until the filter failed due to high aerosol penetration as measured with a downstream photometer or when the pressure drop reached the fan limit of 50 in. WC.

An example of a particle loading test under ambient conditions is shown in Figure 4 where $\text{Al}(\text{OH})_3$ powder is loaded on a RC filter.

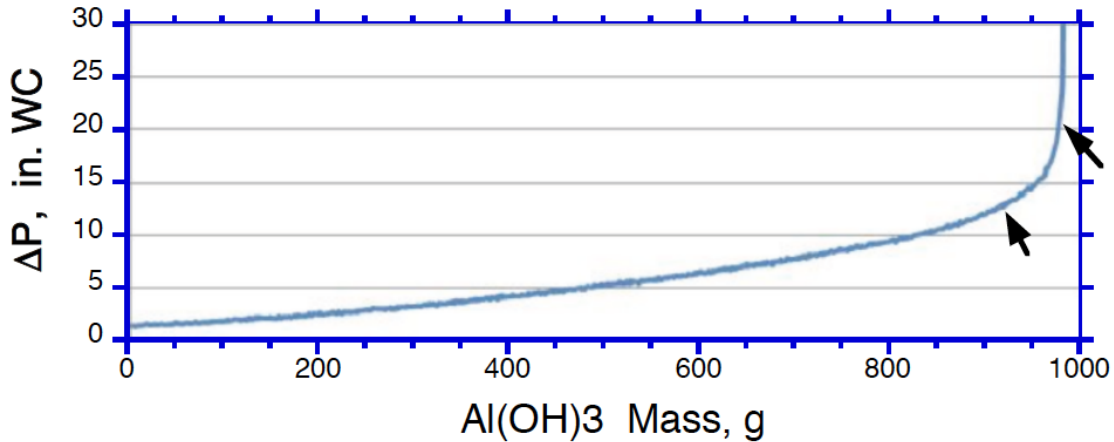


Figure 4. Mass loading curve for a remote change filter loaded with aluminum hydroxide, $\text{Al}(\text{OH})_3$. The arrows indicate the approximate start (12.9 in. WC) and end (20.5 in. WC) of the pleat collapse. The mass of $\text{Al}(\text{OH})_3$ at 4 in. WC is 370 g. The filter run ID is RC-DS1-001 (Giffin et al, 2012)

The differential pressure (DP) across the filter at a constant 2,000 acfm increases steadily as seen in Figure 4 until the ΔP reaches 12.9 in. WC. At that point, the HEPA filter shows a rapid increase in ΔP due to pleat collapse. The pleat collapse is complete at 20.5 in. WC and significantly increases the pressure drop because the effective filter area is dramatically reduced while maintaining the same air flow rate.

Figure 5 shows a series of video frames taken at different stages of filter loading from Figure 4. The video is positioned inside the filter housing and enables monitoring of the exit side of the filter pleats during test conditions. The filter pleats are open at 4 in. WC as seen in Figure 5 (A) where the separations between adjacent pleats are seen as dark regions between the dimple pleats that act as separators. As the DP increases to 10 in. WC in Figure 5 (B) the pleat separations are nearly closed. When the filter reaches a DP of 20 in. WC in Figure 5 (C) all of the pleats are in contact as seen by the disappearance of the dark lines. Finally at 32 in. WC in Figure 5 (D), the filter tears near the sealant and causes some of the pleats to balloon out.

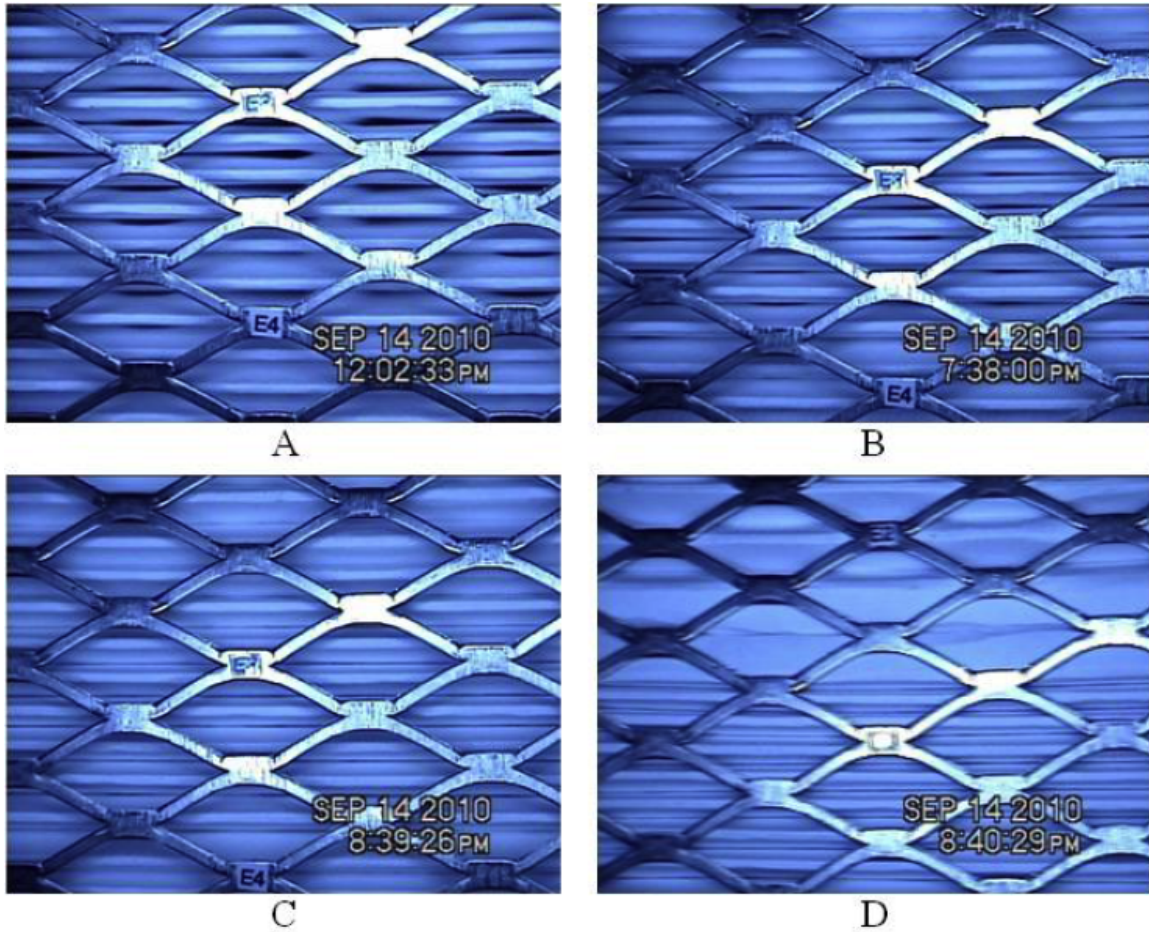


Figure 5. In-testing video images of the filter exhaust side in test RC-DS1-001 at (A) 4 in. WC, (B) 10 in. WC, (C) 20 in. WC, (D) 32 in. WC. (Giffin et al, 2012)

An example of the $\text{Al}(\text{OH})_3$ powder loading on a SC filter is shown in Figure 6.

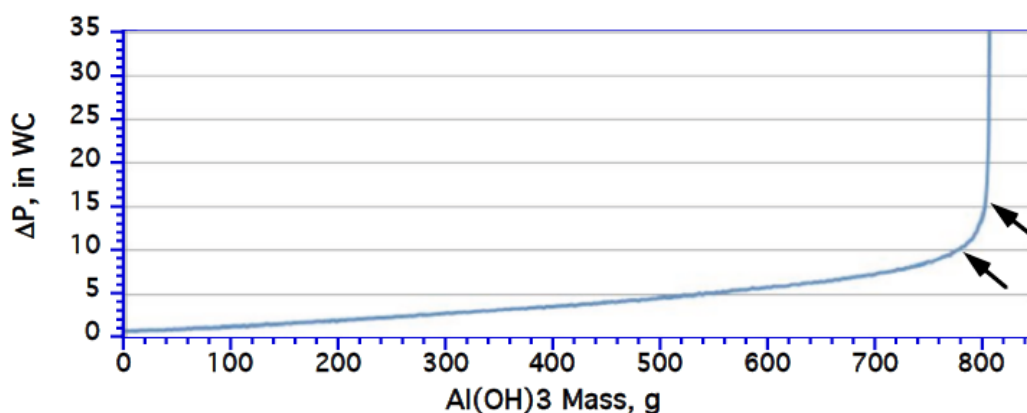


Figure 6. Mass loading curve for a safe change filter loaded with aluminum hydroxide, Al(OH)_3 . The arrows indicate the approximate start (10.2 in. WC) and end (15.6 in. WC) of the pleat collapse. The mass of Al(OH)_3 deposits at 4 in. WC is 440 g. The filter run ID is SC-DS1-001 (Giffin et al, 2012)

An additional five RC and two SC filters were loaded with test aerosols and the results analyzed in a similar fashion. Table 3 summarizes the results from these loading tests.

Table 3. Pressure drop estimates for the start and end of the pleat collapse determined from the particle loading curves under ambient temperature ($\sim 70^\circ\text{F}$) and relative humidity (40-60% RH). The temperature and RH are the values at pleat collapse, and the range during the test is given in parentheses. (Giffin et al, 2012, 2013; Waggoner, 2012b)

Filter ID	Loading Aerosol	Mass of aerosol, kg	Temp, °F	RH, %	Pleat collapse ΔP , in. WC*	
					Start	End
RC-001	Al(OH)_3	0.981	70 (69-72)	45 (43-50)	12.9	20.5
RC-002	Carbon B	1.196	70 (67-72)	60 (48-61)	11.2	16.9
RC-003	AZ Dust	7.760	68 (68-72)	45 (40-65)	12.6	16.1
RC-007	Al(OH)_3	0.974	72 (69-72)	47 (45-52)	13.6	20.0
RC-008	Carbon B	1.070	76 (68-77)	43 (40-59)	10.9	16.0
RC-009	AZ Dust	7.268	68 (67-71)	48 (40-61)	11.9	15.7
SC-001	Al(OH)_3	0.808	70 (70-72)	50 (48-52)	10.2	15.6
SC-002	Carbon B	0.874	72 (68-73)	57 (55-64)	8.8	12.1
SC-003	AZ Dust	5.361	73 (70-73)	50 (50-56)	8.5	12.3

*Visual estimates from the particle loading graphs.

The values of the filter pressure drop at the start and end of pleat collapse were obtained by visual estimates of the loading graphs and have an uncertainty due to judgment errors and errors in extracting data from graphs, especially the DP values

for the start of pleat collapse. Since simple analytic approaches such as taking the first and second derivatives of the graphs would not help identify the start and end of pleat collapse due to the nature of the graph, such approaches were not pursued.

Table 3 shows the ΔP values for the start and end of the pleat collapse are greater for the RC filters than the start and end of the pleat collapse for the SC filters. The tighter filter pack for the RC filters appears to make the RC filter less prone to pleat collapse than the SC filters. A higher pressure drop is required for the RC filter at both the start and end of the pleat collapse compared to the pressure drop required for the SC filter.

Table 3 also shows that the ΔP for both the start and end of the pleat collapse is greater when the RC and SC filters are loaded with $\text{Al}(\text{OH})_3$ powder compared to the comparable ΔP values when loading with carbon black or Arizona Road Dust. The $\text{Al}(\text{OH})_3$ deposit appears to form a more rigid deposit on the filter than the deposits of carbon black and Arizona Road Dust because both the SC and RC filters require a higher ΔP to have pleat collapse. The more rigid deposit absorbs some of the pressure drop that would be transmitted through the deposit layer to the filter medium.

The data in Table 3 was analyzed by first grouping the data into separate categories: SC or RC and start or end using all the loading data; SC or RC and start or end using all the loading data except for $\text{Al}(\text{OH})_3$. A key assumption in the analysis was that the variation of data within each group is random. The ΔP values in each group are then placed in ascending order and assigned a cumulative probability, P_c , value given by $(N_0 - 0.5) / N_T$, where N_0 is the order number of the ΔP value and N_T is the total number of ΔP values. For example, the fourth of 6 ΔP values in a particular group would have a cumulative probability of $(4 - 0.5) / 6 = 0.583$. The ordered number pairs of $(\Delta P, P_c)$ are then fitted to a normal distribution using Kalaidagraph software. A similar fit can be obtained with Excel by first converting the probability fraction to the normalized form using the Excel function $\text{NORMSINV}()$ with the cumulative probability in the argument. The trend curve is then obtained by the best linear fit to of the ΔP values versus the NORMSINV values.

The graphical results from analyzing the data in Table 3 when grouped according to SC or RC and pleat Start or End are shown in Figure 7. Figure 7 shows the RC filters require a higher ΔP for pleat collapse compared to the SC filters for both the start of the pleat collapse and the end of the pleat collapse. However, the influence of the higher ΔP for the $\text{Al}(\text{OH})_3$ loading tests at both the start and end of pleat collapse is included in the results. To separate out the effect of the high ΔP due to the $\text{Al}(\text{OH})_3$ deposits, Table 3 is reordered in Table 4.

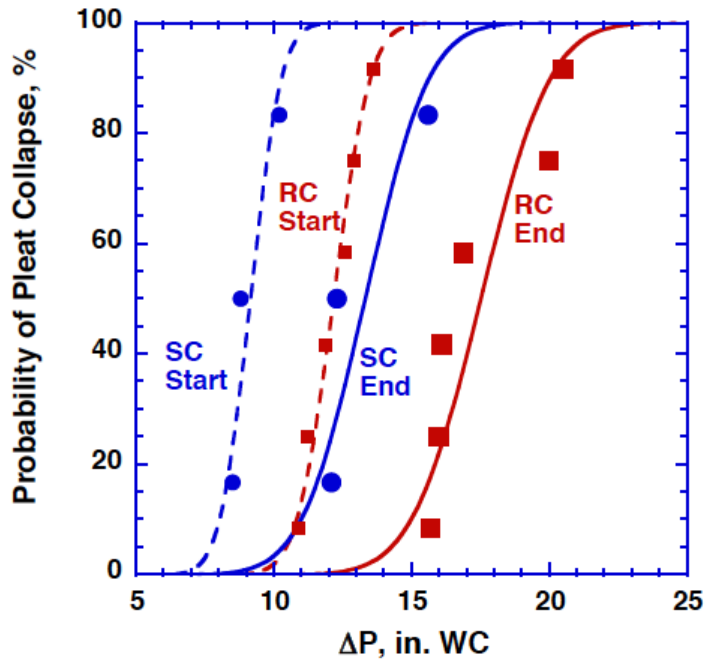


Figure 7. Probability of the start and end of pleat collapse as a function of the filter ΔP for the Flanders SC and RC radial flow HEPA filters using all the data in Table 3.

Table 4. Reordering of Table 3 to separate effects of filter design and test dust on start and end of pleat collapse.

Filter	Al(OH) ₃		Carbon Black		Arizona Road Dust	
	Start	End	Start	End	Start	End
RC	12.9	20.5	11.2	16.9	12.6	16.1
RC	13.6	20.0	10.9	16.0	11.9	15.7
SC	10.2	15.6	8.8	12.1	8.5	12.3

Table 4 shows that the ΔP values for the carbon black and Arizona Road Dust loading at the start and end of the pleat collapse are similar and significantly lower than the comparable ΔP values for the Al(OH)₃ loading. Thus a logical grouping would combine the carbon black and Arizona Road Dust data for the RC and SC filters and compare these graphs to the graphs for the Al(OH)₃ loading. Using the analysis method described, the probability data and curves are obtained as shown in Figure 8.

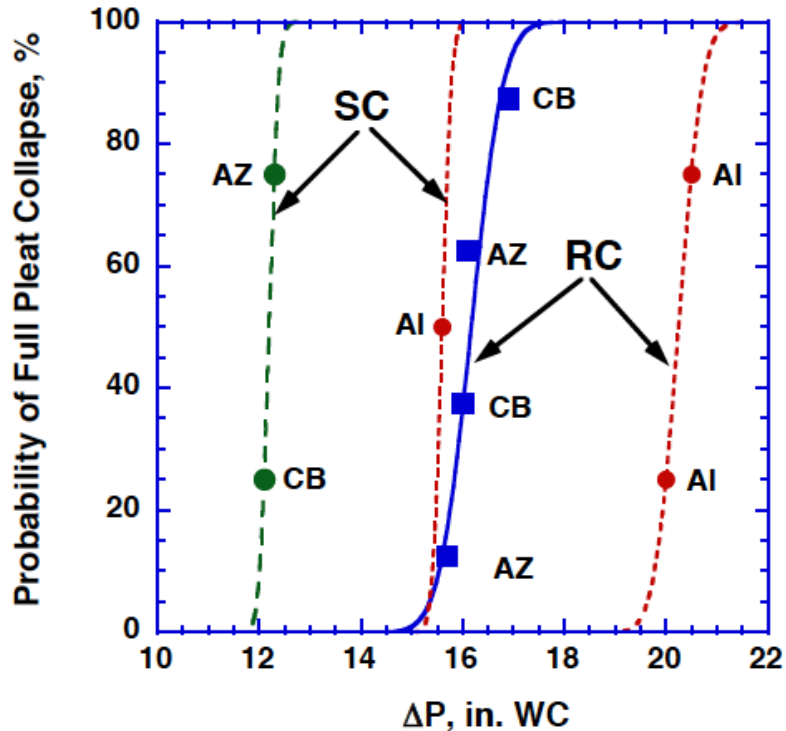


Figure 8. Probability of full pleat collapse for the Flanders RC and SC filters at room temperature and relative humidity with the $\text{Al}(\text{OH})_3$ data isolated. The ΔP at final pleat collapse at 50% probability for the SC and RC filters without the $\text{Al}(\text{OH})_3$ data are 12.2 and 16.2 in. WC respectively. The curve for the single $\text{Al}(\text{OH})_3$ test for the SC filter is based on the SC curve for the AZ and CB tests.

The much higher ΔP values for the $\text{Al}(\text{OH})_3$ in Figure 8 are attributed to the rigid $\text{Al}(\text{OH})_3$ deposits that have a portion of the deposit ΔP that does not transmit to the filter medium for pleat displacement. A rigid particle deposit structure prevents the full DP to be applied to the filter medium and thus leads to erroneously higher DP values for pleat collapse.

The DP values for full pleat collapse at 50% probability values from Figure 8 are tabulated in Table 5. The difference in ΔP between the $\text{Al}(\text{OH})_3$ loading and the CB and AZ loading is 3.4 in. WC for the SC filter and 4.0 in. WC for the RC filter. However the SC filter only has 0.804 kg deposit at pleat collapse (Figure 6) compared to 0.98 kg for the RC filter at pleat collapse (Figure 4). When this difference in mass deposit of $\text{Al}(\text{OH})_3$ is considered, then the pressure drop increment due to the $\text{Al}(\text{OH})_3$ deposits that is not transmitted to the medium is the same for both RC and SC filters as seen in Table 5. The pressure drop increment per mass of $\text{Al}(\text{OH})_3$ deposit is 4.1 and 4.2 for the RC and SC filters respectively.

Table 5. Comparison of pressure drop increment of Al(OH)₃ deposits not contributing to pleat collapse for RC and SC filters.

Filter type	ΔP_1 , in. WC Al(OH) ₃	ΔP_2 , in. WC CB & AZ	$\Delta P_1 - \Delta P_2$, in. WC	M, kg Al(OH) ₃	$(\Delta P_1 - \Delta P_2)/M$
RC	20.2	16.2	4.0	0.98	4.1
SC	15.6	12.2	3.4	0.80	4.2

Photographs of the particle deposits suggest that the Al(OH)₃ deposits are structurally rigid and can have an independent pressure drop that does not transmit to the filter medium. Figure 9 shows photographs of acetylene soot and Al(OH)₃ particle deposits on the inlet side of fully loaded HEPA filters (Waggoner, 2012a, 2016). Although the HEPA filters are not the same as the Flanders radial flow HEPA filters, the nature of the deposits will be similar.

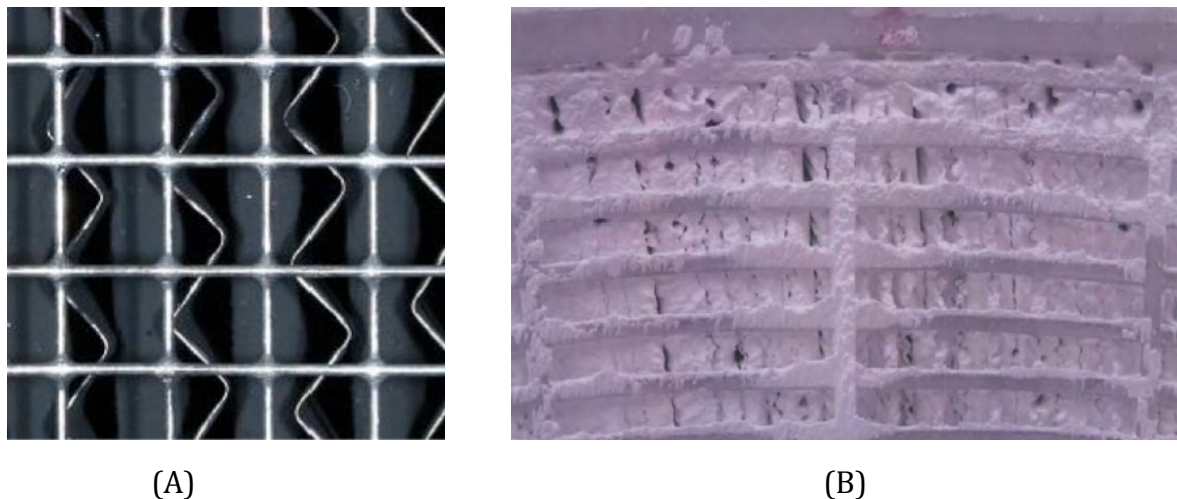


Figure 9. Photographs of (A) acetylene soot and (B) Al(OH)₃ powder deposits on fully loaded HEPA filters. Waggoner (2012a, 2016)

The acetylene soot deposits in Figure 10 (A) show the soot deposits cover the surface of the medium and do not have an independent structure. Thus the pressure drop due to the soot deposits transmit directly to the filter medium. In contrast, the Al(OH)₃ deposits in Figure 10 (B) shows a rigid, cement-like structure filling the filter pleats. Such a rigid particle deposit would have some independent pressure drop that does not transmit to the underlying HEPA medium. Arizona Road Dust (~5 microns) is much larger than Al(OH)₃ powder (1 micron), and therefore less prone to forming rigid structures. The Arizona Road Dust is more sand-like and would transmit the pressure drop from the deposit onto the HEPA filter medium.

Elevated Temperature and Humidity Tests

MSU also conducted tests on two RC and two SC radial flow HEPA filters in which the filters were preloaded under ambient conditions with $\text{Al}(\text{OH})_3$ powder at 2,000 cfm until the filter DP reached 4 in. WC (Giffin et al, 2012). The filters were then subjected to elevated temperature conditions and the pressure drop monitored as a function of time to determine pleat collapse and filter failure (Giffin et al, 2012). The elevated temperature was achieved using a natural gas burner inside the duct inlet. To prevent combustion soot from adding to the filter DP, the burner was operated with no filter in place until the soot was negligible and the test housing became hot. The test filter was then installed in the hot duct and the test commenced. Water was sprayed inside the heated duct to increase the RH as needed. Although no tests or analyses were performed to ensure the water spray had evaporated, no water accumulation was found in the test duct or on the filters. The test results for the three filters are shown in Figures 10-12.

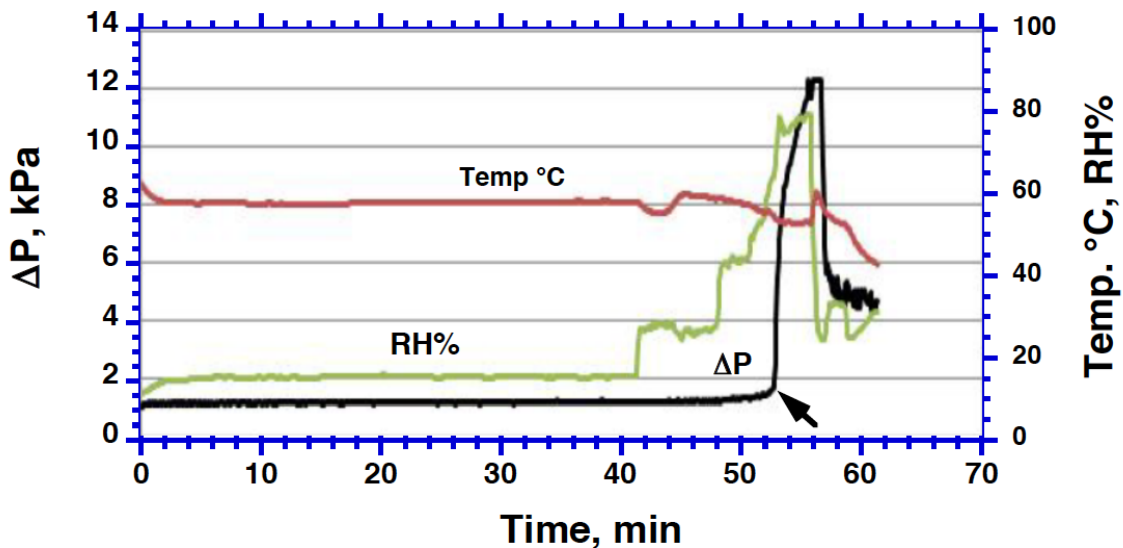


Figure 10. Exposure of filter RC-004 to elevated temperature and increasing RH after pre-loading the filter with $\text{Al}(\text{OH})_3$ to 4 in. WC at 2,000 cfm. The arrow indicates the filter ΔP at which pleat collapse begins and is complete. (Giffin et al, 2012)

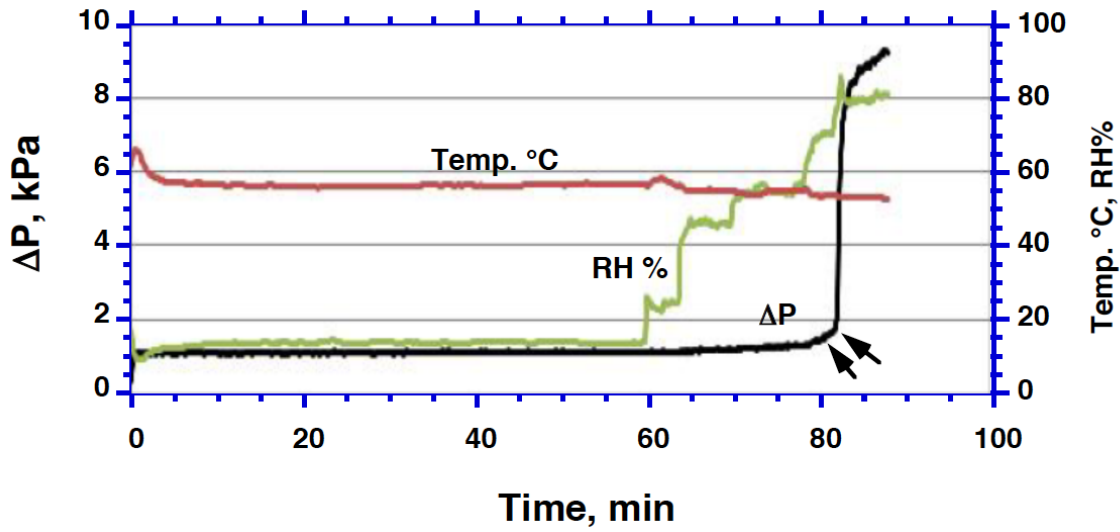


Figure 11. Exposure of filter RC-010 to elevated temperature and increasing RH after pre-loading the filter with $\text{Al}(\text{OH})_3$ to 4 in. WC at 2,000 cfm. The two arrows indicate the filter ΔP at which pleat collapse begins and is complete. (Giffin et al, 2012)

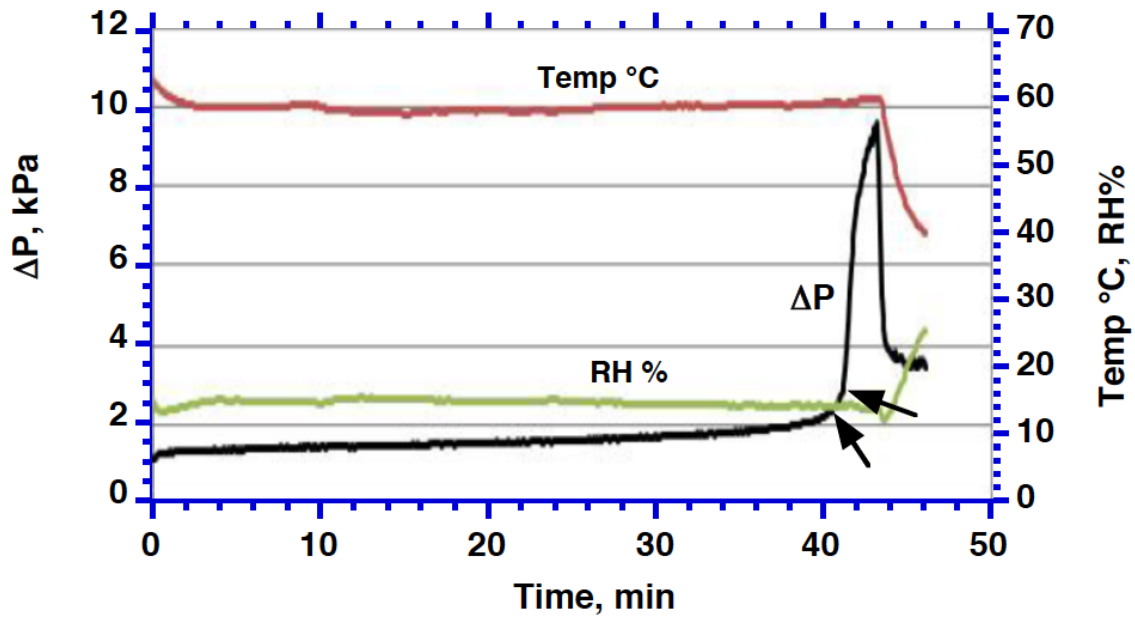


Figure 12. Exposure of filter SC-004 to elevated temperature and low RH after pre-loading the filter with $\text{Al}(\text{OH})_3$ to 4 in. WC at 2,000 cfm. The two arrows indicate the filter ΔP at which pleat collapse begins and is complete. (Giffin et al, 2012)

The test conditions and the ΔP values at the start and end of the pleat collapse from Figures 10-13 are tabulated in Table 6.

Table 6. Pressure drop estimates for the start and end of the pleat collapse determined from exposure to elevated temperature (130- 144°F) after pre-loading the filters with $\text{Al}(\text{OH})_3$ to 4 in. WC. The temperature and RH are at the end of the pleat collapse, and the range during the test is given in parentheses. (Giffin et al, 2012, 2013; Waggoner, 2012b)

Filter ID	Mass, kg $\text{Al}(\text{OH})_3$	Temp, °F at collapse	RH % at collapse	Pleat collapse ΔP , in. WC	
				Start	End
RC-004	0.411	130 (127- 140)	75 (15-78)	6.8	6.8
RC-010	0.375	129 (128- 137)	79 (14-85)	6.2	7.2
SC-004	0.459	137 (136- 139)	14 (13-15)	8.8	11.3

Table 6 shows that the SC filter has a slightly larger ΔP for pleat collapse than the RC filters at the elevated temperature test with $\text{Al}(\text{OH})_3$ loading. The opposite trend was observed in Tables 3 and 4 and in Figure 8 for loading with $\text{Al}(\text{OH})_3$ powder and the other two aerosols at ambient temperatures.

The data in Table 6 was analyzed using the same procedure described previously for filter loading under ambient temperature conditions. Figure 13 shows the resulting graphs of probability of pleat collapse at the start and completion of the pleat collapse at elevated temperature.

Since the filters in Figure 13 were preloaded with $\text{Al}(\text{OH})_3$ powder prior to the elevated temperature and relative humidity exposure, the issue of a rigid particle deposit raises the concern that the ΔP value at pleat collapse could be lower than that indicated. The primary argument against that possibility is that the particle loading in the elevated temperature tests is less than half that in the ambient temperature tests as seen in Tables 3 and 6. Without sufficient mass of $\text{Al}(\text{OH})_3$ deposits, it would not be possible to form the deposit seen in Figure 9B where the deposit covers the pleat inlets. The deposits that bridge the pleat inlets are supported by the pleat ends and would have a portion of the deposit ΔP transmitted to the pleat ends and not contribute to the deflection of the flat medium within the pleats to collapse the pleats. Photographs of intermediate deposits on the filter would readily confirm this assessment.

Such an assessment is supported by the ΔP versus mass curves in Figures 4 and 6 for the RC and SC filters respectively. The moderate deposit of $\text{Al}(\text{OH})_3$ falls at about the mid-point of the near linear ΔP curve. This suggests that the deposit is

uniformly distributed over the filter medium; and, thus, the ΔP across the particle deposit is applied directly to the medium and contributes to pleat collapse.

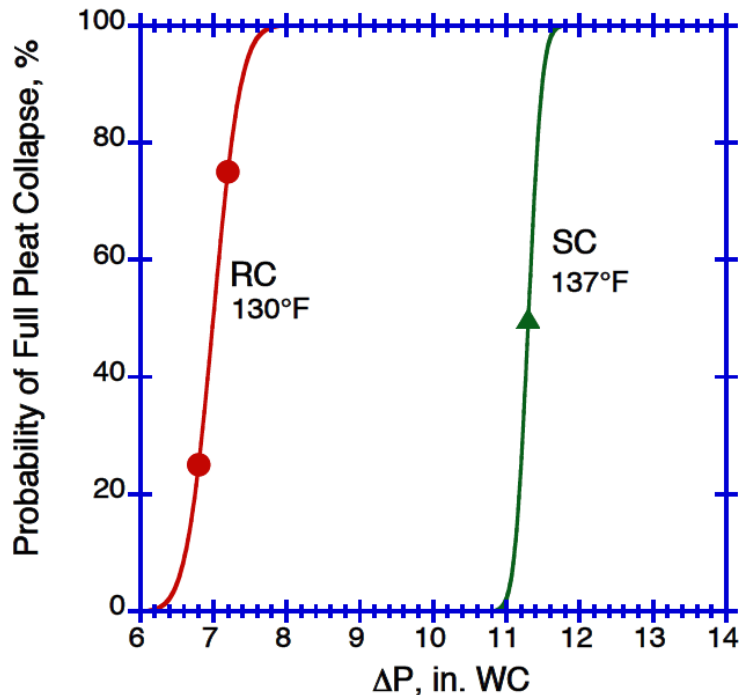


Figure 13. Probability of full pleat collapse as a function of filter pressure drop for Flanders SC and RC radial flow HEPA filters at elevated temperature taken from Table 6. The curve drawn through the single point was taken from the SC filter at ambient conditions in Figure 8.

Summary of Radial Flow HEPA Filter Test Results

The tests from Figures 8 and 13 are combined and shown in Figure 14.

Figure 14 shows that as the temperature is increased from about 70°F to 130-137°F, the ΔP value for pleat collapse decreases dramatically for the RC filters and only slightly for the SC filter. This decrease is due to the softening of the medium at elevated temperature whereby the medium is less stiff and more easily deflected to cause pleat collapse. The dramatic decrease in the ΔP for pleat collapse seen for the RC filter is due to the tight packing (Table 1) of the pleats whereby a small deflection of the medium results in pleat collapse. The SC filter already has a lower ΔP value for pleat collapse due to the loose pleat packing (Table 1) and is only slightly enhanced by softening the medium with higher temperature

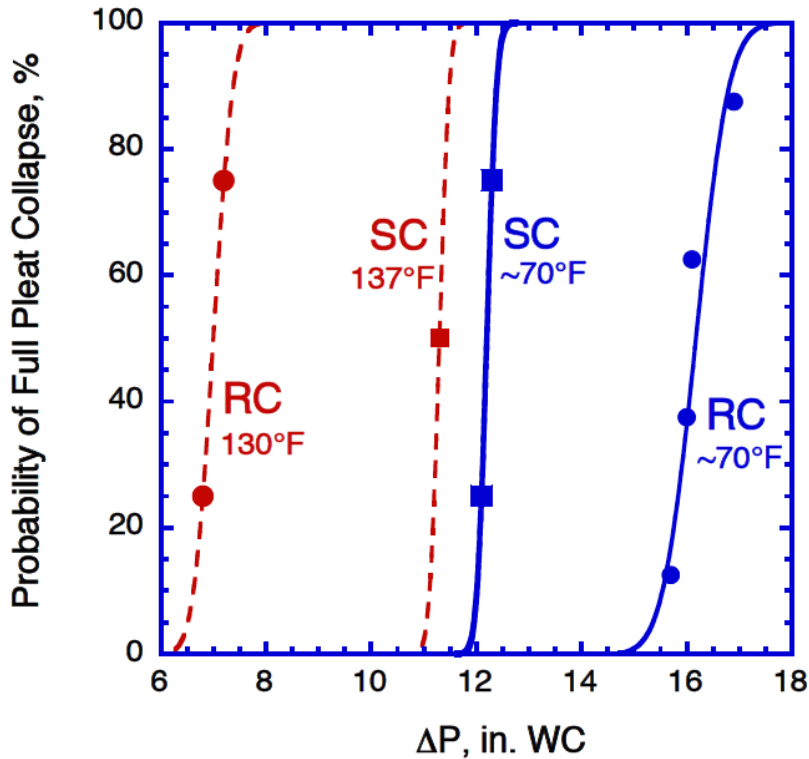


Figure 14. Probability of final pleat collapse as a function of filter pressure drop for Flanders radial flow HEPA filters at room temperature and elevated temperature from Figures 8 and 13 respectively.

The pleat collapse for both ambient and elevated temperature is characterized as having a critical ΔP_c where the filter ΔP quickly increases in an unstable feed-forward process. Once the ΔP_c is reached, the pressure drop causes the pleat spacing to decrease, thereby increasing the filter ΔP , which, in turn, causes the pleat spacing to decrease further and thereby increases the filter ΔP further in the unstable collapse process. If the filter is close to the ΔP_c , then any process that increases filter ΔP past the ΔP_c can initiate the pleat collapse. Potential processes include a transient increase in air flow that results in increasing the filter ΔP and an increase in the ΔP of the $\text{Al}(\text{OH})_3$ deposit due to deposited water droplets or adsorbed moisture. At the elevated temperatures in this study (130-137°F), once the ΔP_c is reached, it takes less than 2 minutes for complete pleat collapse.

Figure 15 shows the probability of reaching the ΔP_c for the SC and RC filters is similar to the full pleat collapse in Figure 14 but at lower ΔP values.

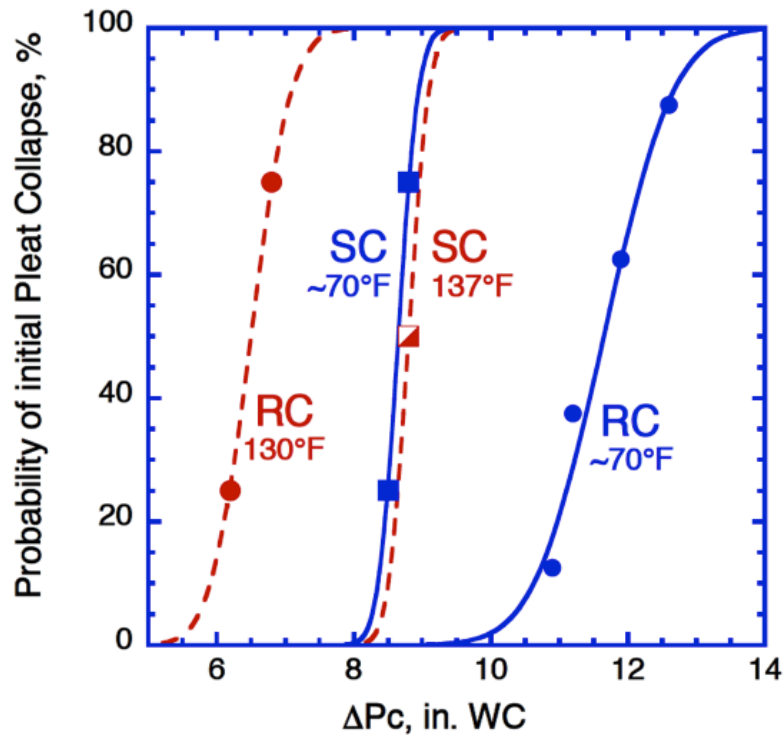


Figure 15. Probability of initial pleat collapse (ΔP_c) as a function of filter pressure drop for Flanders radial flow HEPA filters at room temperature and elevated temperature.

Based on the analysis of the radial flow HEPA filters described here, there are two filter design characteristics that determine the value of the DPC: (1) the tightness of the filter pack and (2) the separation of the medium within the pleats. These two characteristics produce opposite effects on the pleat collapse. Table 1 shows that the SC filter has a looser filter pack (lower ppi) than the RC and therefore has pleat collapse at lower ΔP values. However the tighter filter pack has a smaller pleat spacing and therefore requires less deflection of the medium for pleat collapse. From Figures 14 and 15, the SC filter pack is sufficiently loose that the ΔP_c does not change and the final DP at pleat collapse decreases slightly with increasing temperature. In contrast, the RC filter has a major reduction in the ΔP_c and final ΔP with increasing temperature.

Pleat Collapse with Radial Flow HEPA Filters

A small number of tests have shown that axial flow HEPA filters also exhibit pleat collapse (Waggoner, 2012a; Stormo et al, 2016). Although ten Flanders separatorless HEPA filters were tested, six with the DYN-E2 design (U-pack) and four with the Pureform design (W-pack), data on the filter DP at pleat collapse was only available for two of the U-pack filters (Stormo et al, 2016). Figures 16 and 17 show the filter ΔP , temperature, and RH as a function of time for the U-pack filters preloaded with $\text{Al}(\text{OH})_3$ to 4 in. WC at 1000 cfm and 1500 cfm respectively and then exposed to elevated temperature at 1000 and 1500 cfm.

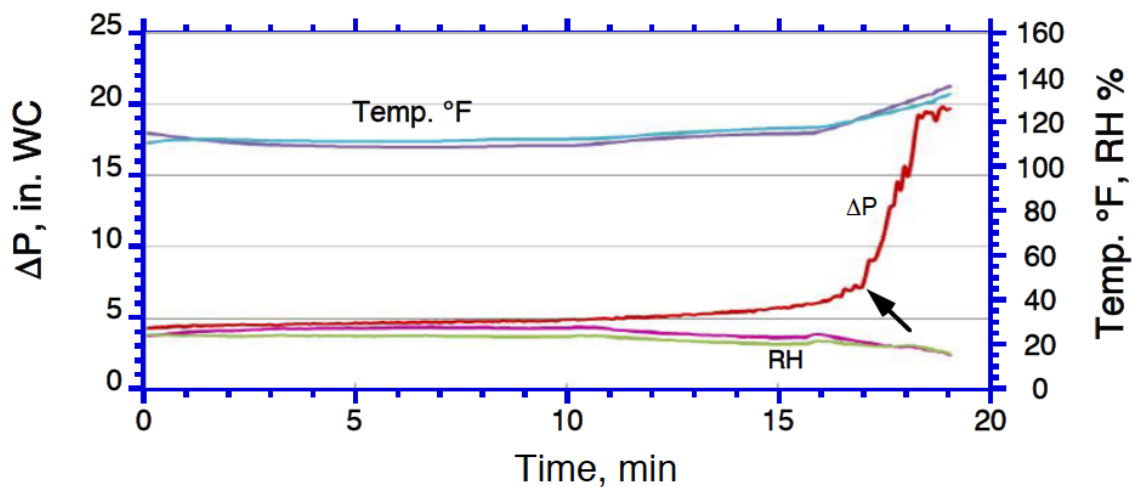


Figure 16. Test data for a 24 x 24 x 11.5 inch Section FC Axial Flow Flanders U-pack HEPA Filter loaded to 4 in. w.c. dP with $\text{Al}(\text{OH})_3$ followed by exposure to elevated temperature at the rated flow of 1000 cfm. The arrow marks the start of pleat collapse. (Waggoner, 2012a; Stormo et al, 2016)

The initial pleat collapse in Figure 16 occurs at 7.3 in. WC, 122 °F, 20% RH, and 17 minutes.

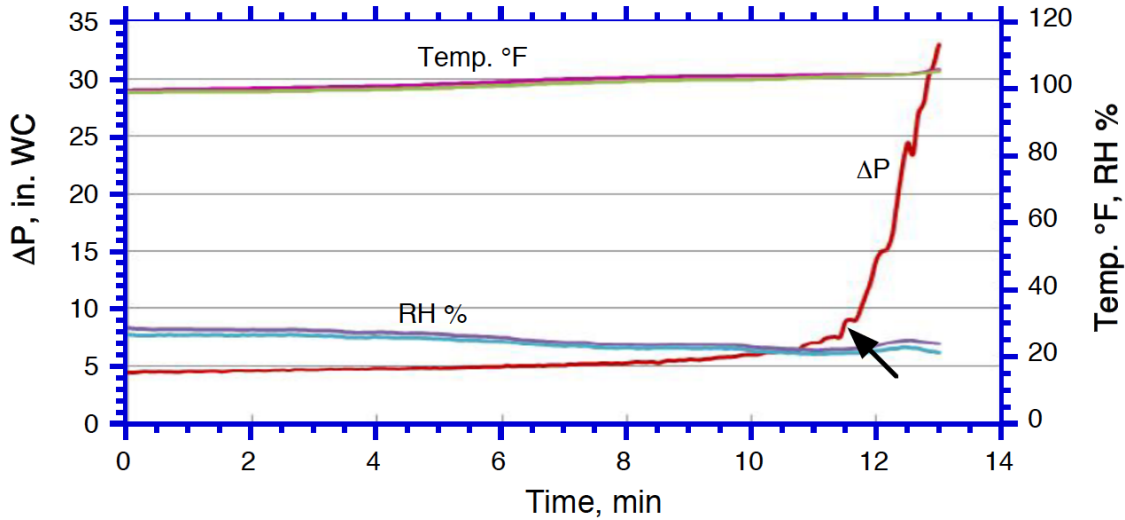


Figure 17. Test data for a 24 x 24 x 11.5 inch Section FC Axial Flow Flanders U-pack HEPA Filter loaded to 4 in. w.c. dP with $\text{Al}(\text{OH})_3$ followed by exposure to elevated temperature and relative humidity at the rated flow of 1500 cfm. The arrow marks the start of pleat collapse. (Waggoner, 2012a; Stormo et al, 2016)

The initial pleat collapse in Figure 17 occurs at 8.4 in. WC, 104 °F, 22% RH, and 11.6 minutes.

Comparing the pleat collapse in axial flow HEPA filters in Figures 16 and 17 with the radial flow HEPA filters in Figures 10-12 shows the start of the pleat collapse occurs at much shorter times (11.6 and 17 minutes compared to 40-80 minutes) and at lower temperatures (104 and 122°F compared to 129-137°F). The U-pack filters also have slower rate of pleat collapse (as measured by the rate of ΔP increase versus time) than the radial flow HEPA filters.

The pleat collapse does not seem to correlate with relative humidity. The U-pack filters show pleat collapse at low RH values (20% and 22%) while the radial flow filters show pleat collapse at both low (14% RH in Figure 12) and high (75% and 79% RH in Figures 10 and 11 respectively) relative humidity.

A more detailed analysis of the pleat collapse with axial flow HEPA filters was not possible with the limited data available.

Effect of Relative Humidity on Pleat Collapse

From the test results shown in Figures 10 and 11 for the radial flow filters, one is tempted to conclude that increased moisture is also responsible for pleat collapse in addition to elevated temperature. The RC filters pre-loaded with $\text{Al}(\text{OH})_3$ powder at elevated temperature showed no increase in ΔP until a water spray was turned on to increase the relative humidity. Once the RH reached 80%, the filters rapidly increased in ΔP due to pleat collapse. There is a strong prejudice to consider elevated humidity as responsible for the pleat collapse since it is well known that both the tensile strength and stiffness of the glass fiber medium decreases significantly when the medium becomes wet.

However, the rapid increase in filter ΔP with the injected water spray may be due to an abrupt increase in air flow due to the fan adjusting to changing temperature while trying to maintain a constant mass flow as observed in preliminary MSU tests (Waggoner, 2012B). Once the critical DP is reached, the filter quickly has pleat collapse in less than 2 minutes. Figure 10 show significant changes in air temperature when the water spray was turned on, and Figure 11 shows small temperature changes when the water spray is turned on. Unfortunately, MSU did not report the air flow during these transients to clarify the source of the increase in filter ΔP .

To help understand the effect of high humidity on filter pleat collapse, all of the initial pressure drop data for the radial flow HEPA filter used in Figure 15 plus the additional two pressure drops for the U-pack filters in Figures 16 and 17 are graphed in Figure 18 as a function of the relative humidity at pleat collapse. The temperature at pleat collapse are also shown in Figure 18. Unfortunately, the data is not sufficient to make any statements regarding the effect of moisture on pleat collapse (Giffin et al, 2012).

The analysis of the SC and RC filters showed that the filters have significantly different values of ΔP_c and that the RC filters are sensitive to temperature while the SC filters are not. The U-pack filter also appears to have a temperature dependency, but with only two data points, there is little confidence in any speculation.

Although the MSU data is insufficient to clarify the dependency of pleat collapse on the relative humidity, other studies have shown that there is negligible increase in filter ΔP with exposure to elevated relative humidity up to 80% for both clean filters and filters loaded with room dust (Rudinger et al, 1985). The lack of ΔP increase indicates that the filter and particle deposits have not adsorbed water.

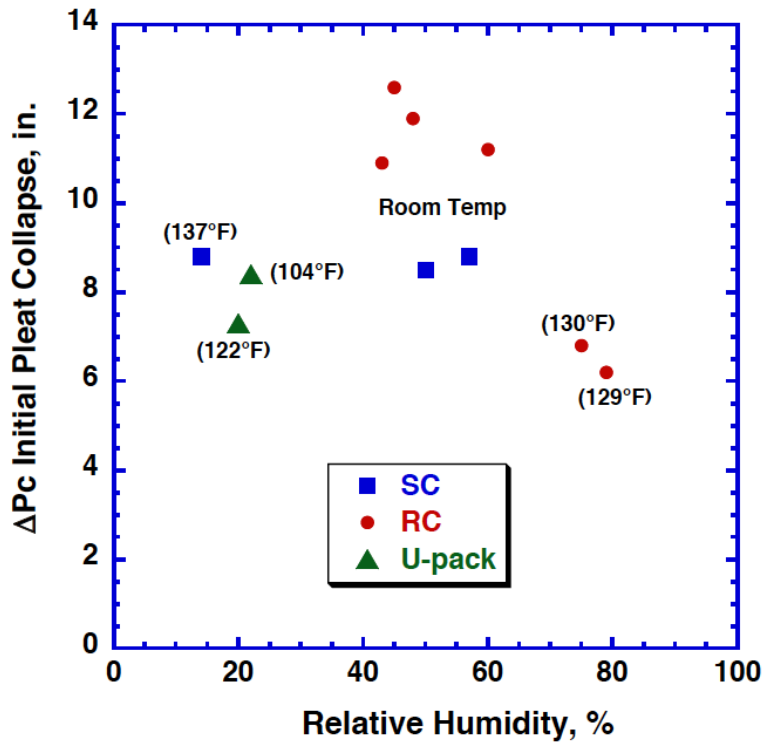


Figure 18. Plot of the initial ΔP at pleat collapse (ΔP_c) as a function of the relative for the 10 data points for SC and RC filters from Figure 15 plus the two additional points for the U-pack filters from Figure 16 and 17 .

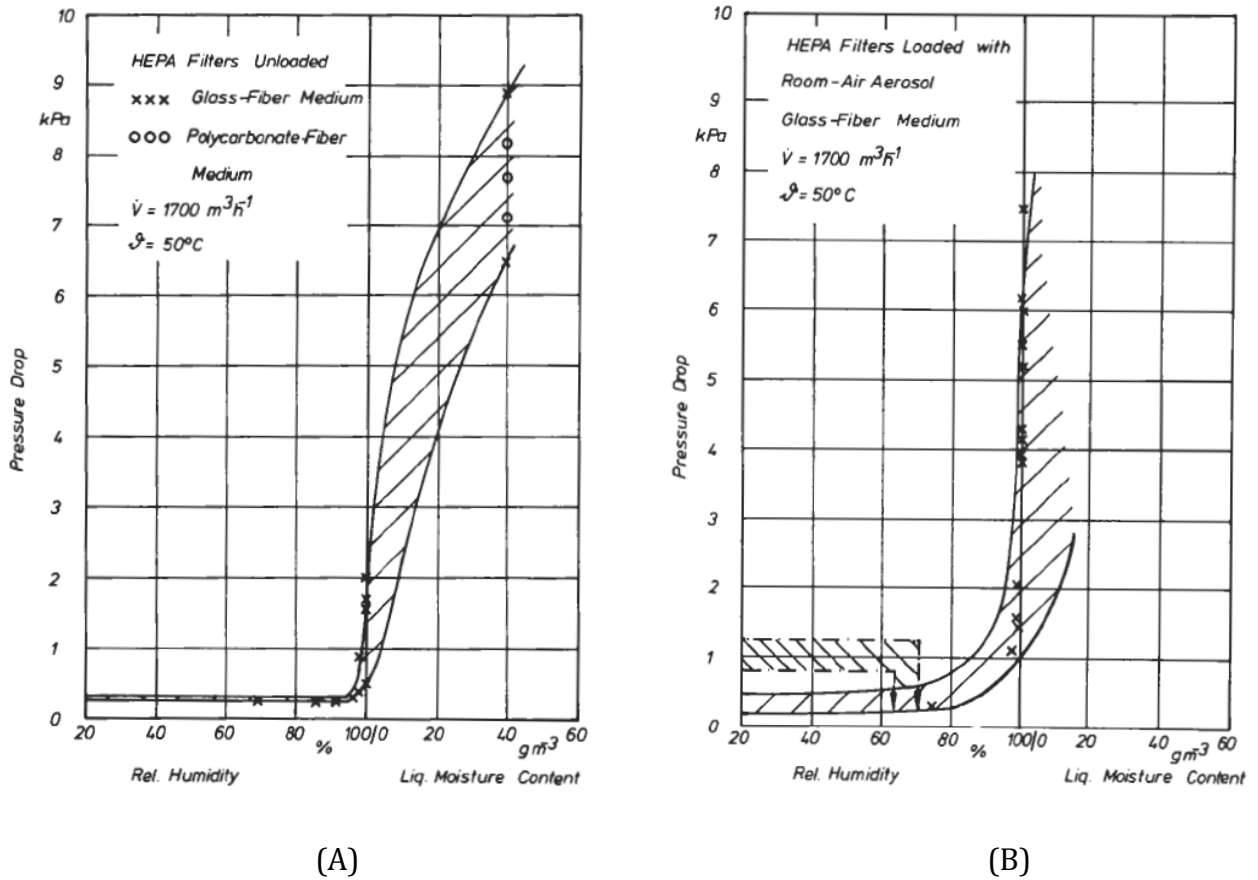


Figure 19. Adsorption of moisture on (A) clean HEPA filters and on (B) HEPA filters loaded with room air dust have little or no impact on the filter ΔP below 80% relative humidity. The filters are nuclear grade, 1000 cfm, glass fiber HEPA filters with aluminum separators. (Rudinger et al, 1985)

Plate Deflection Model of Pleat Collapse

The collapse of filter pleats in Figure 1B can be simulated with the mechanical deflection of two sheets of medium that represents the two side of a pleat. The deflection of sheets of material from uniform forces (i.e. applied pressure) can be computed from stress-strain analysis and properties of the material. The formulas for the deflection of rectangular sheets by a uniform force are derived by Young and Budynas (2002)

For a uniform pressure the medium sheet has a maximum deflection of

$$y_{P,\max} = \frac{\alpha_P P W^4}{E t^3} \quad (1)$$

where

- $y_{P,\max}$ = maximum deflection in center, inches
- α_P = a constant that depends on the D/W ratio,
- W = width between separator peaks or embossments, inches
- D = pleat depth, inches
- P = applied pressure on the sheet, pounds/ inch²
- E = Modulus of elasticity (Young's modulus), pounds/inch²
- t = thickness of medium, inches

The values of α_P are a function of the D/W ratio of the sheet and are given in Table 7 (Young and Budynas, Table 11.4 (2002))

Table 7. Values of α_P coefficients as a function of D/W

D/W:	1.0	1.2	1.4	1.6	1.8	2.0	3.0	4.0	5.0	∞
α_P	0.0444	0.0616	0.0770	0.0906	0.1017	0.1110	0.1335	0.1400	0.1417	0.1421

The dimensions of the medium sheet to be tested depends on the design of the filter. The key filter parameters to be used in the deflection tests are given in Figure 20. Here t = medium thickness (inches), D = pleat depth (inches), 2X = space between the two sides of the pleats (inches), and N = number of pleats per inch.

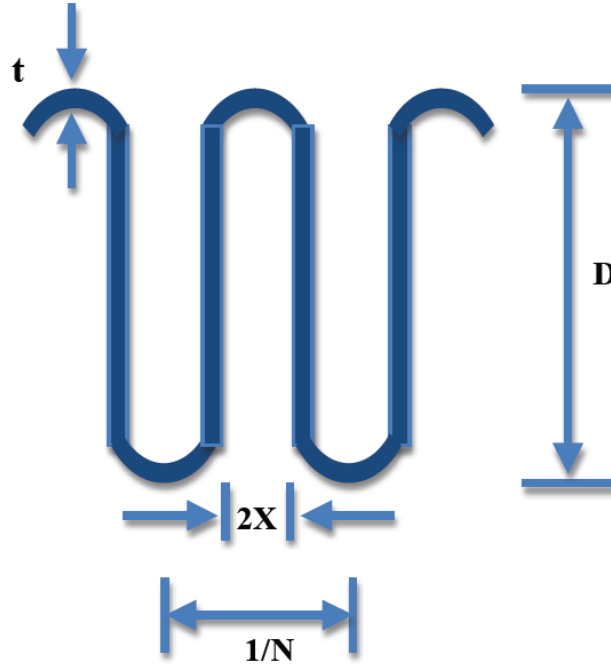


Figure 20. Key filter parameters used for pleat collapse testing. t = medium thickness (inches), D = pleat depth (inches), $2X$ = space between the two sides of the pleats (inches), and N = number of pleats per inch.

Note that the distance of one pleat is $1/N$. Thus from Figure 20, we have

$$\frac{1}{N} = 4X + 2t \quad (2)$$

Rearranging Equation 2 yields,

$$X = \frac{1}{4N} - \frac{t}{2} \quad (3)$$

Figure 20 and Equation 3 are only applicable to axial flow HEPA filters. The comparable drawing for radial flow HEPA filters is shown in Figure 21.

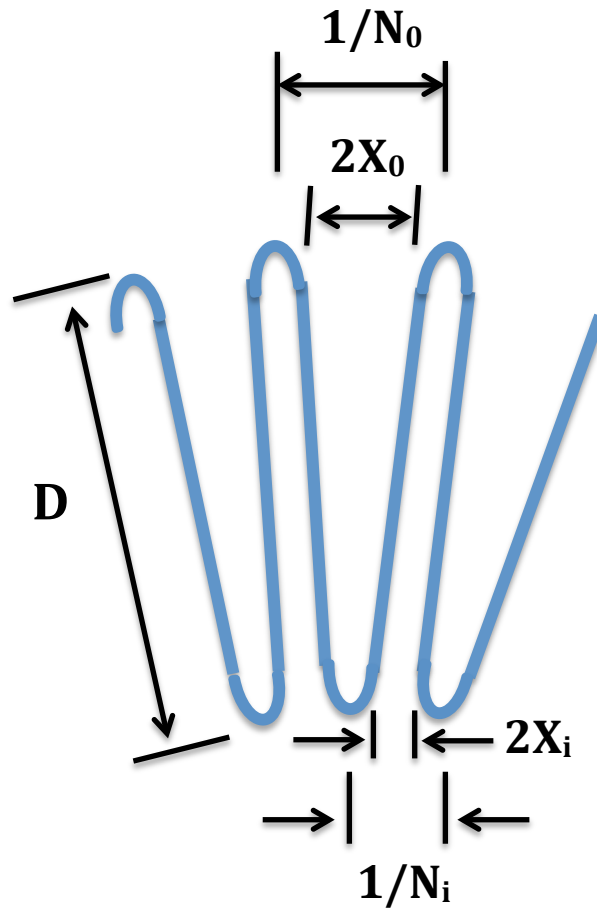


Figure 21. Drawing for the pleat configuration in radial flow HEPA filters.

Due to the asymmetry of the radial flow pleats, the inlet and outlet pleat parameters are different as shown in Figure 21. The inlet pleats are tightly spaced while the outlet pleats are more widely separated. The inlet channel width is shown in Figure 21 as constant along the pleat depth, D . This follows from the manufacturing process of pleating the medium to produce a flat filter pack. When the filter pack is wrapped around into a cylinder, the pleats naturally form the accordion shape shown in Figure 21, with a constant inlet pleat channel width and an expanding outlet pleat channel width. For the Flanders dimple pleat design, the pleat asymmetry is less pronounced because the embossed portions of the medium can be slightly compressed when forming the cylindrical filter pack.

To avoid the complexities of the asymmetrical inlet and outlet of the radial flow HEPA, the average of the inlet and outlet pleats per inch are used. Assuming the average $N = 6.85$ and 6.34 pleats/inch for the Flanders remote-change and safe-change designs, and $t = 0.018$ in., then Equation 3 yields $X = 0.0275$ in. and 0.0304 in. for the Remote-Change and Safe-Change designs respectively. Thus deflections of the medium by 0.0275 in. and 0.0304 in. represents a complete pleat collapse for RC and SC filters.

The dimensions of the pleat section to be used in Equation 1 can be determined from the cut open pleat section shown in Figure 3C. Since the consecutive embossments are into and out of the plane, the width, W , of the sheet is determined by the distance between the first and third embossments, or $W=1.36$ in.. Each pleat section thus has a center embossed ridge that adds rigidity to the sheet. The length of the pleat section is the depth of the pleat, or $D= 3$ in.. The value of α_p for $D/W= 2.21$ from Table 7 is $\alpha_p =0.1157$ with interpolation.

Equation 1 can be used to determine the effective modulus of elasticity, E , using the filter pressure drop at final pleat collapse and the parameter values determined here. Figure 22 shows the results of this calculation as a function of temperature.

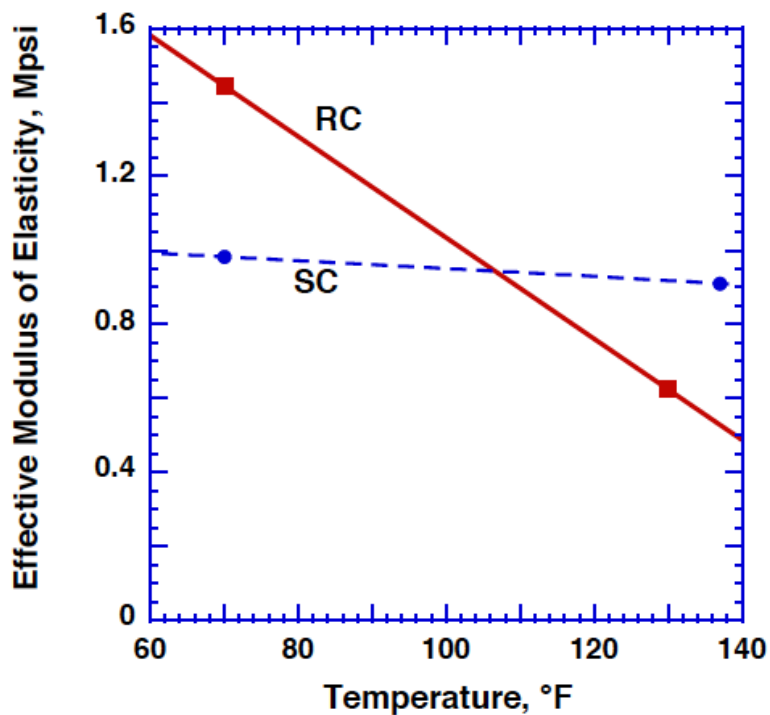


Figure 22. Computed effective modulus of elasticity for the SC and RC filter as a function of temperature.

Note that the computed modulus of elasticity depends not only on the intrinsic material properties of the glass fiber medium, but also the embossments defining the medium sheet, the additional embossment in the center of the sheet, and the tightness of the filter pack. Further analysis of pleat collapse on different designs of separatorless HEPA filters (e.g. U-pack, W-pack, mini-pleat) will be required to allow a separation of the filter pack design from the intrinsic modulus of elasticity of the HEPA filter medium.

Filter Medium Tears

When the HEPA filter experiences higher pressure drops or the filter becomes wet, then the filter media may tear. Two different failure modes have been identified with medium tears in HEPA filters: (1) bending of the filter pack with tears of the medium perpendicular to the pleats and (2) ballooning of pleat end and tearing along the pleat.

Tears Due to Bending of the Filter Pack

Figure 23 illustrates the medium tears that result from bending of the HEPA filter pack for filters without a guard screen.

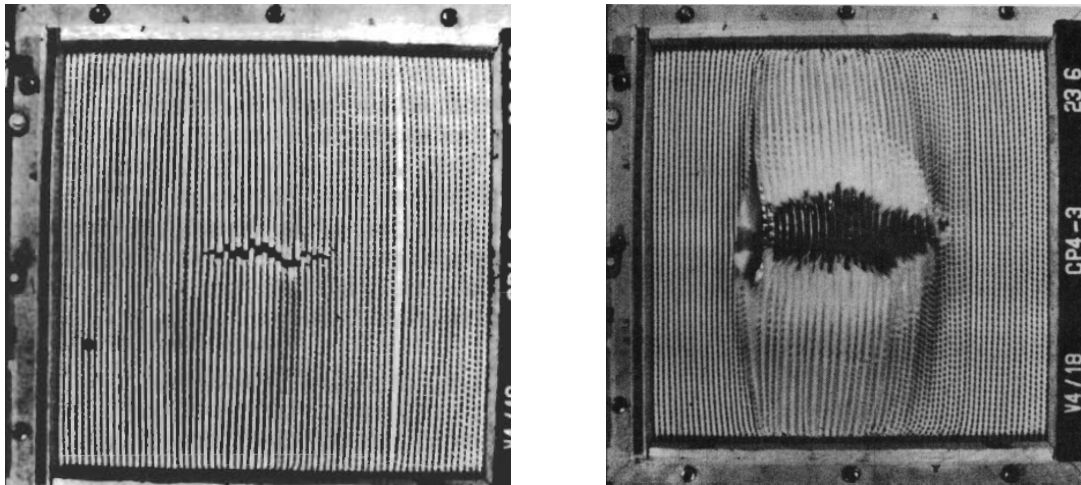


Figure 23. Failure of a new 24 in. x 24 x 11.5 in. deep-pleated HEPA with aluminum separators rated at 1,000 cfm due to bending of pleats under high flow with dry air. (Rudinger et al, 1987).

Note the breakage occurs at the center of the filter, where the pressure drop forces the filter pack to bulge out and the strain is the greatest. Such breakage would not occur when a screen is used and prevents the filter from bulging. The breakage would occur closer to the filter pack sealant as shown in Figure 24.

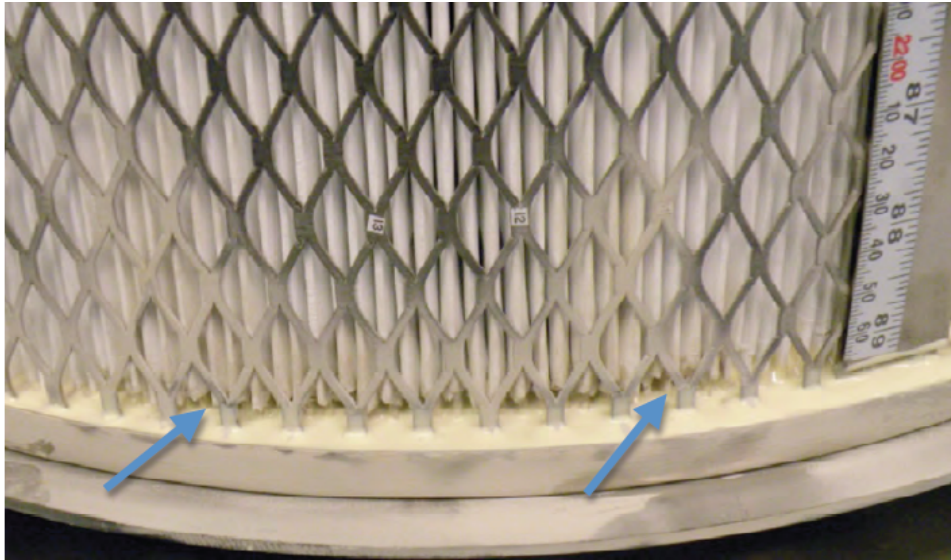


Figure 24. Close-up photo of remote change, radial flow HEPA filter, RC-009, loaded with Arizona Road Dust to high pressure drop. The filter suffered complete pleat collapse at 15.7 in. WC and (Table 3) and ruptured at 40 in. WC at 2000 cfm dry air flow. The arrows show the region of the media where the pleats are torn loose from the sealant (shown as yellow). (Waggoner et al, 2012b)

The bending force on the filter pack in Figure 24 is the greatest near the sealant where the filter pack is secured but does not have the support of the protective screen.

The bending of HEPA filter packs and the subsequent medium tears has also been seen with filters using ribbon separators as shown in Figure 25. The screen prevents the filter pack from bulging out in the center, thus placing the greatest strain near the end cap where the filter pack is secured with the urethane sealant. The pressure drop forces the filter pack to bulge toward the support screen. The ribbon separator of the filter pack makes contact with the screen a small distance from the end cap and remains fixed. Between this fixed point and the urethane sealant, the filter bulges and has no support. Note that the medium tear occurs at the edge of the ribbon separator in Figure 25 B, where the thickness of the ribbon separator exacerbates the already high stress in the filter pack and causes the medium tears.

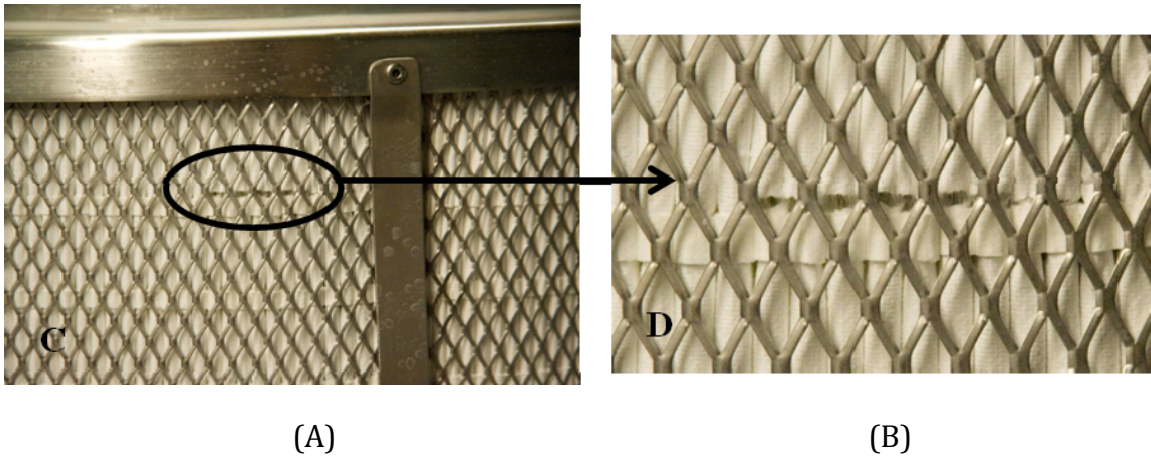


Figure 25. Failure of Vokes radial flow HEPA filter with ribbon separators due to bending of the filter pack following particle loading at 2,000 cfm dry air. (Giffin et al, 2012).

For separator filters, the separator prevents the complete collapse of the filter media. However, separator filters also have media tears at higher pressures as seen in Figures 26 and 27. Figures 26 and 27 show that the separatorless HEPA filters fail at significantly lower pressure drops than filters with separators.

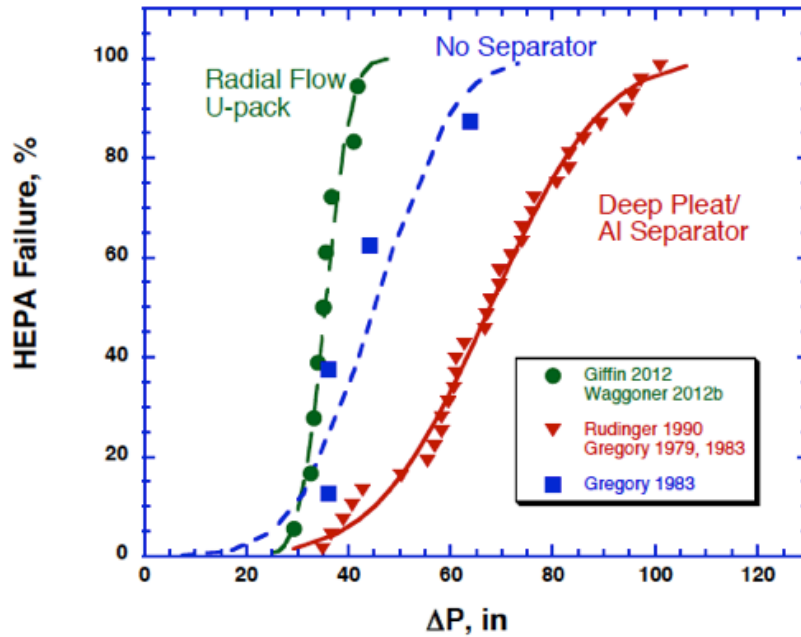


Figure 26. Failure of HEPA filters due to media tears as a function of DP for three different filter designs tested at ambient temperature and RH and high aerosol loading at constant flow or high air flows : dimple pleat radial flow (Giffin et al 2012, 2013), axial flow separatorless (W-pleat) and mini-pleat with string separator (Gregory et al, 1983), and axial flow deep-pleated with aluminum separators (Rudinger, 1990, Gregory, 1979, 1983). Note that Gregory et al (1983) lumped together the mini-pleat filter and the separatorless (W-pleat) filter.

Note that although the three different filter designs have different ΔP failure curves, they all converge to a threshold failure value about 25-30 in. WC.

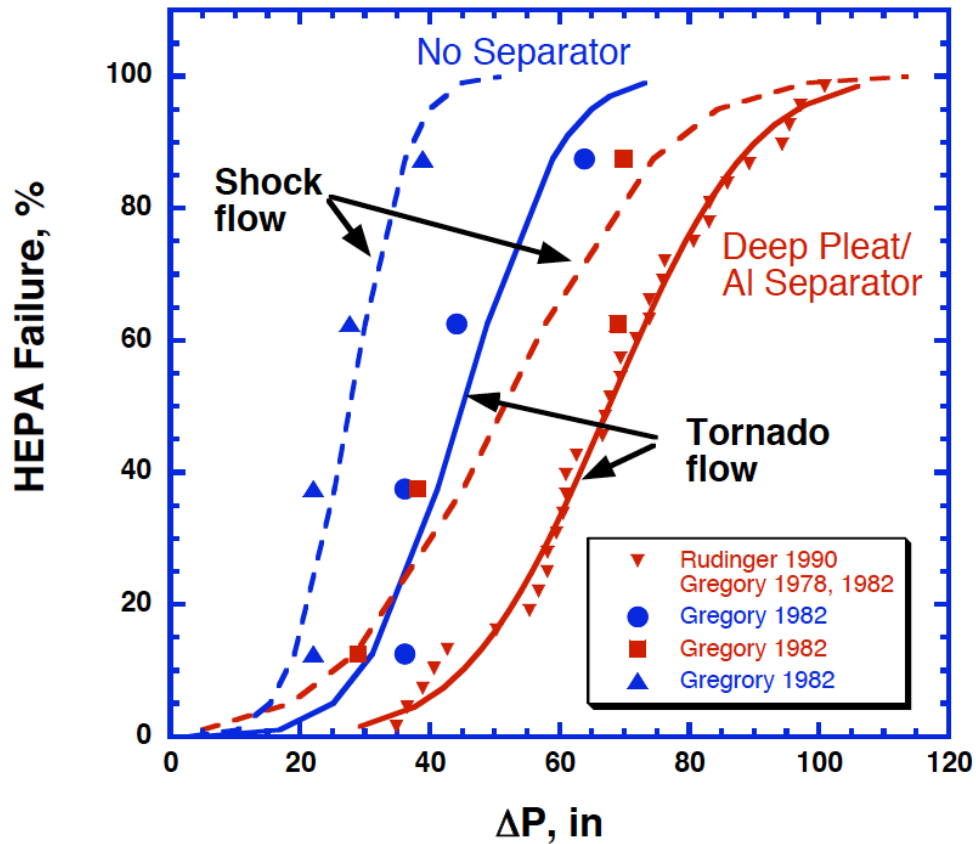


Figure 27. Failure of HEPA filters due to media tears as a function of ΔP for separator and separatorless filter designs tested at ambient temperature and RH: axial flow separatorless (W-pleat) and mini-pleat with string separator (Gregory et al, 1983), and axial flow deep-pleated with aluminum separators (Rudinger, 1990, Gregory, 1979, 1983). Note that Gregory et al (1983) lumped together the mini-pleat filter and the dimple pleat (W-pleat) filter.

Note that all of the examples of medium tears given in Figures 23-27 have occurred in dry air streams. If the filter becomes wet then the inherent tensile of the HEPA medium decreases significantly, and filter medium tears at far lower filter ΔP values as shown in Figure 28.

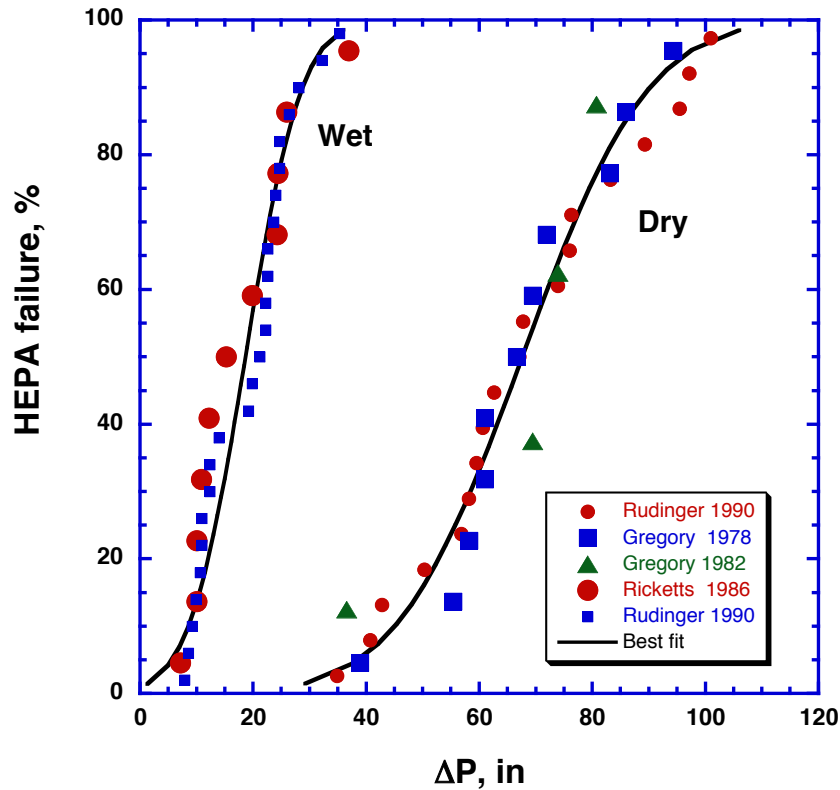


Figure 28. Failure of HEPA filters due to media tears as a function of DP for deep pleated filters with aluminum separators at ambient temperature and either ambient RH (dry) or with high humidity (wet). Note that the wet test differs from that used in the MSU tests or in the AG-1 test, and the wet curve does not represent a constant moisture challenge.

The procedure by Ricketts (1987) and Rudinger (1990) to determine the ΔP at failure for the wet conditions consisted of raising the RH of the rated air flow at 122°F from 50% to 100% until failure was observed. If HEPA failure did not occur, then additional water was sprayed onto the filter until a rupture occurs. The added water increased the filter pressure drop. Unfortunately, the moisture challenge at HEPA failure was not recorded.

Rudinger et al (1987) developed a theory to explain the medium tears due to bending of the filter pack. Figure 28 shows the basic concept of the bending of the filter pack and the resulting tensile stress on the downstream side of the filter.

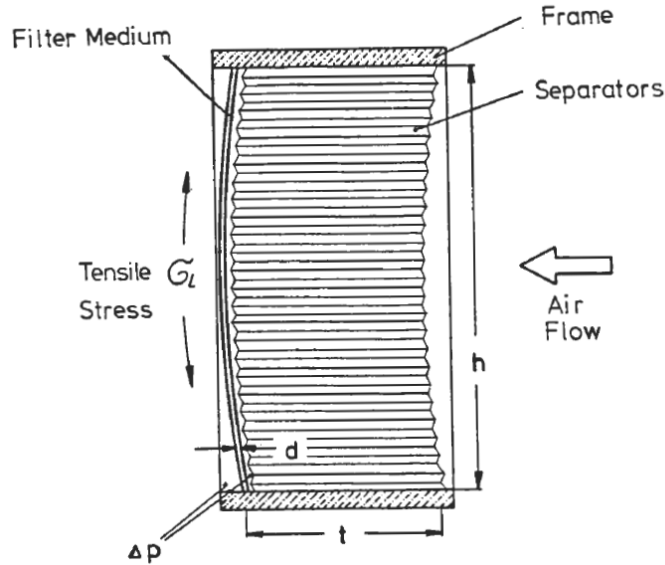


Figure 29. Drawing of the deflection of the filter pack with high differential pressure that induces a tensile stress on the downstream filter pleats and results in medium tears perpendicular to the pleat direction. (Rudinger et al, 1987)

The theory of medium tears due to filter pack deflection is based on examining the stress on a single pleat using general concepts from bending of beams (Rudinger et al, 1987, 1990). Figure 30 shows a sketch of a single pleat that is deflected due to high pressure. The theory of the medium stress due to pleat deflection developed by Rudinger et al (1987, 1990) is given by Equation 4.

$$\sigma_L = \left(\frac{W H^2}{4 A t D^2} + \frac{2 p}{t \sqrt{\epsilon}} \right) \Delta P \quad (4)$$

where

σ_L	=	the tensile stress on the filter medium
W	=	width of the HEPA filter pack
H	=	height of the HEPA filter pack
D	=	depth of the medium pleats
t	=	thickness of HEPA filter medium
p	=	pitch of the separator corrugation
ϵ	=	elongation of the medium due to loading in %
ΔP	=	pressure drop across the HEPA filter pack

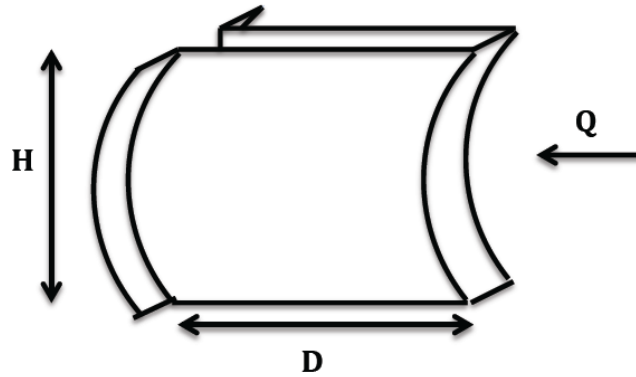


Figure 30. Schematic of a single pleat of a HEPA filter pack that is deflected due to high pressure drop. The Q represents the air flow against a pleat of height, H, and depth, D.

Rudinger et al (1990) demonstrated that Equation 4 gave good agreement with experimental HEPA filter failures under both dry and humid air conditions in Figure 31.

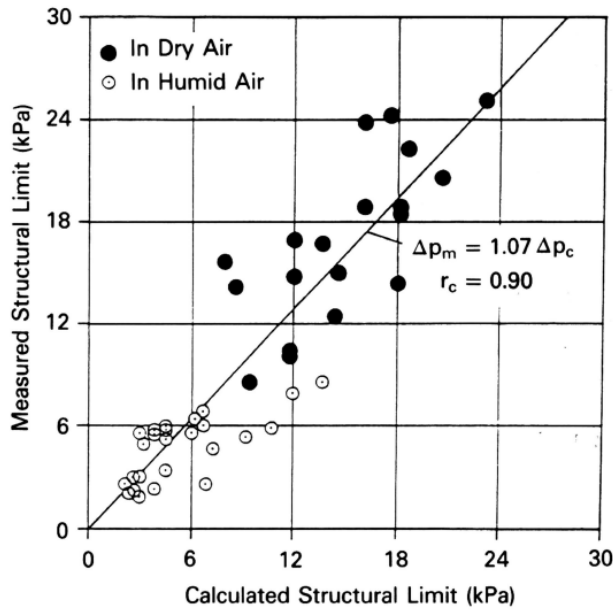


Figure 31. The comparisons of measured structural strength (filter ΔP) and calculated structural strength (filter ΔP) using Equation 4 for both dry air and humid air tests show good agreement.

Tears Due to Swelling and Rupture of Pleat Ends

Another major failure mode that results in medium tears is the swelling and rupture of pleat ends in both dry and wet environments. Filter designs that have the pleats loosely packed are more prone to have pleat swelling than tightly packed pleats. The pleat ruptures occur in both dry air conditions as shown in Figure 32 and in wet conditions as shown in Figure 33.

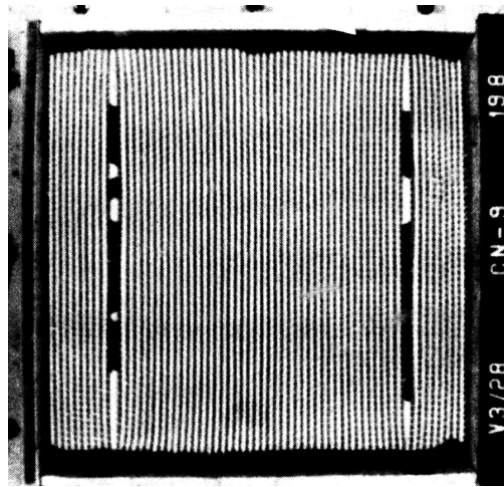


Figure 32. Example of a clean 1000 cfm HEPA filter subjected to high DP under dry air conditions that suffered pleat swelling and rupture (Rudinger et al, 1990).



Figure 33. Example of a clean 1000 cfm HEPA filter that suffered pleat rupture following exposure to the ASME AG-1 resistance to pressure test under wet conditions.

Pleat tears frequently occur in filters that have failed the ASME AG-1 wet overpressure test. The AG-1 resistance to pressure test requires the filter be exposed to air flow at 95°F, 95% RH and additional water spray such that the resulting filter pressure drop is 10 inches WC. Since the test does not measure the air flow, it is not possible to determine if pleat collapse occurs. Failure is defined as having a 0.3 micron DOP efficiency of less than 99.97% at 20% rated flow following one hour exposure at the elevated temperature and moisture. Thus the test only measures filter tears and cannot measure pleat collapse. The results for several different filters, including the W and U pack filters, are shown in Figure 34 (Sen et al, 2010).

A key finding in the Sen (2010) paper is that the HEPA failures of the AG-1 test are statistical as shown by the cumulative failure distribution in Figure 34. Thus the AG-1 practice of testing 4 filters suggests that the filter has less than 25% (1/4) probability of failing the wet pressure test. A review of the Flanders AG-1 resistance to pressure test indicates that the failure rate for W pack filters is 17% (4/24) and for U pack is 0% (0/8). Although the 0% failure for the U pack is likely due to the small number of tests and may be greater with more tests, it is clear that the W pack is more prone to tear failure than the U pack. This follows not only because of the test results in Figure 34, but also because the media tears are due to weaker tensile strength. The W pack filters have the pleats formed by bending over the embossed media whereas the U pack filters have pleats formed by bending over flat media. Bending over an embossment puts a large stress on the media and makes it prone to tearing.

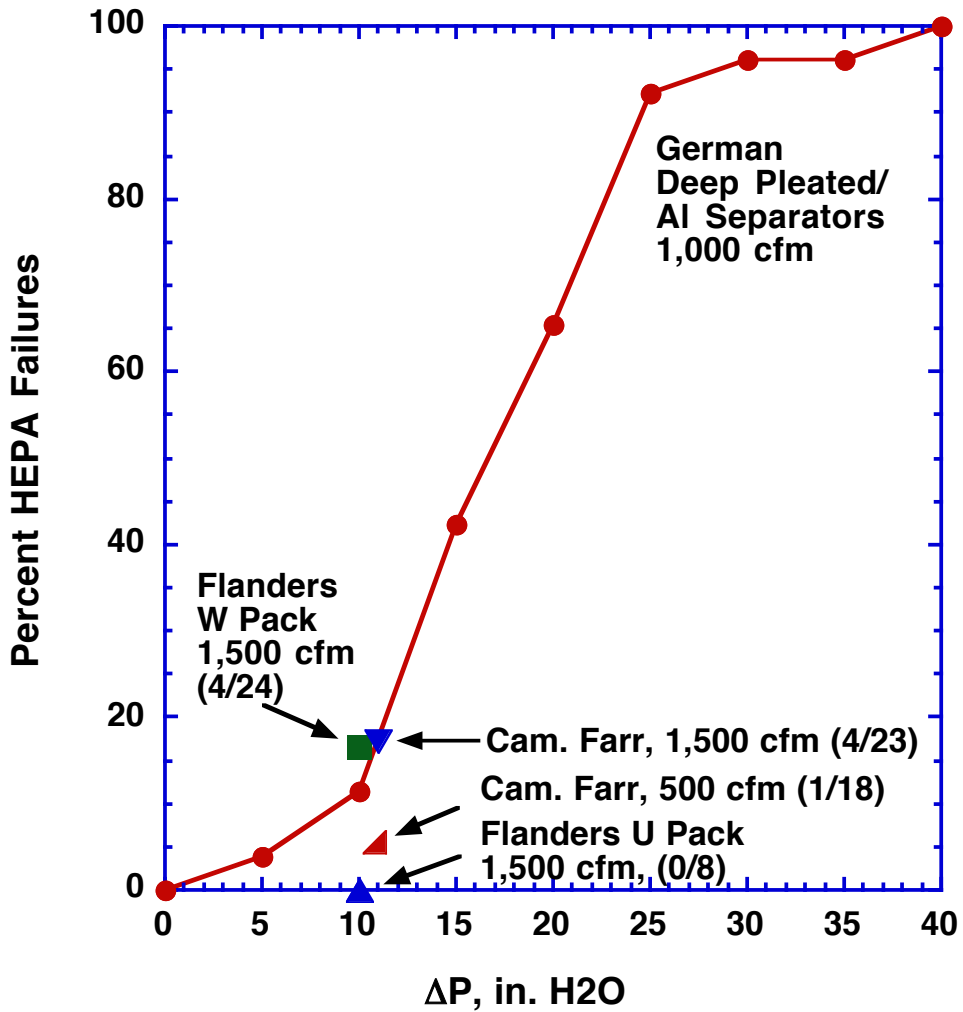


Figure 34. Percent of HEPAs failing the AG-1 resistance to pressure test superimposed on a curve for percent failures of German HEPA filters due to torn filter media (Ricketts et al, 1987) exposed to moist air at increasing pressure drops. The numbers in parentheses are the number of failed filters over the total number of tested filters. (Sen, 2010).

Rudinger et al (1987, 1990) also developed the theory for HEPA filter failure due to pleat swelling and rupture as shown in Figure 35.

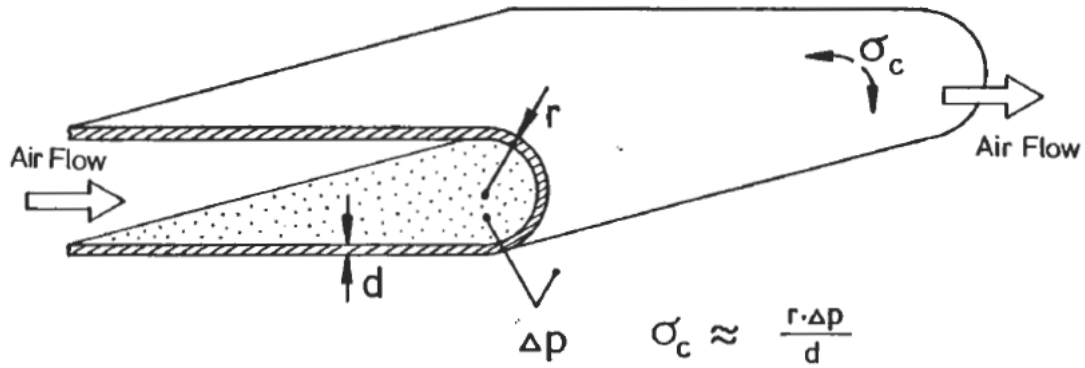


Figure 35. Sketch of filter pleat showing the critical tensile strength, σ_c , for pleat swelling and rupture is dependent on the product of the pleat radius of curvature, r , and the filter pressure drop divided by the medium thickness.

Comparison of the experimental DP at failure with computed failures show reasonable agreement in Figure 36.

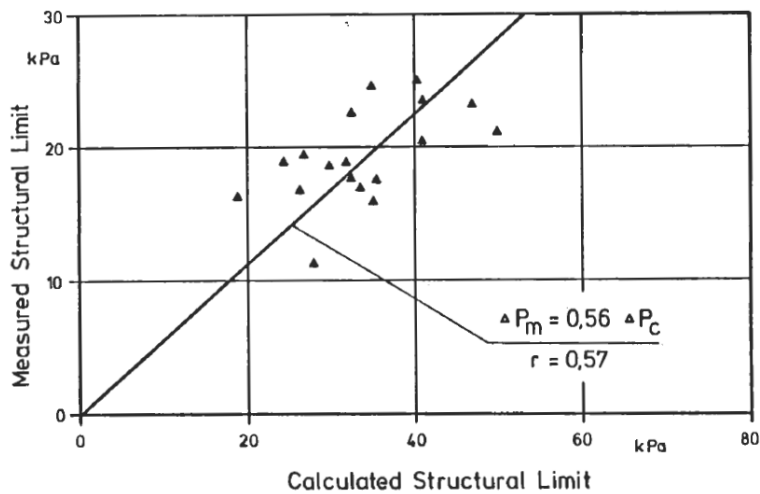


Figure 36. Comparison of measured and calculated filter DP at pleat failure show good agreement. (Rudinger et al, 1987)

Ricketts et al (2004) continued to further refine the models for HEPA filter failure due to filter pack bending and pleat rupture.

References

- Giffin, P.K., Parsons, M.S., Wilson, J.A., and Waggoner, C.A. (2012) "Performance comparison of dimple pleat and ribbon separated radial flow HEPA filters" 32nd Nuclear Air Cleaning Conference, June 17-19, 2012, Denver, CO, International Society for Nuclear Air Treatment Technologies, www.isnatt.org
- Giffin, P., Waggoner, C., and Parsons, M. (2013) Lifecycle testing results of dimple pleat radial flow HEPA filters under ambient and elevated conditions, *Aerosol Science and Technology*, Vol 47, No. 7, pp. 785-791.
- Gregory, W.S., Andrae, R.W., Duerre, K.H., Horak, H.L., Smith, P.R., Ricketts, C.I., and Gill, W (1979) Air cleaning systems analysis and HEPA filter response to simulated tornado loadings, Proceedings of the 15th Nuclear Air Cleaning Conference, pp. 694-706. www.isnatt.org
- Gregory, W.S., Martin, R.A., Smith, P.R. and Fenton, D.E. (1983) Response of HEPA filters to simulated accident conditions, Proceedings of the 17th DOE Nuclear Air Cleaning Conference, pp. 1051-1068. CONF-820833. www.isnatt.org
- Munson, B.R., D.F. Young, and T.H. Okiishi (2006) *Fundamentals of Fluid Mechanics*, Fifth Edition, John Wiley & Sons.
- Ricketts, C.I. and Smith, P.R. (2004) "A model for the stresses in the filter medium of Deep-Pleat HEPA filter packs and its practical applications." In Proceedings of 28th Nuclear Air Cleaning Conference. www.isnatt.org
- Rudinger, V, Ricketts, C.I., and Wilhelm, J.G.(1985) Limits of HEPA-filter application under high-humidity conditions" Proceedings of the 18th DOE/NRC Nuclear Air Cleaning Conference, M.W. First, Editor, CONF-840806, Vol. 2. pp 1058-1084. www.isnatt.org
- Rudinger, V, Ricketts, C.I., Wilhelm, J.G., and Alken, W. (1987) Development of glass-fiber HEPA filters of high structural strength on the basis of the establishment of the failure mechanisms" Proceedings of the 19th DOE/NRC Nuclear Air Cleaning Conference, M.W. First, Editor, NUREG/CP-0086, CONF-860820, Vol. 2. pp 947-966. www.isnatt.org
- Rudinger, V, Ricketts, C.I., Wilhelm, J.G. (1990) High-Strength, High-efficiency particulate air filters for nuclear applications, *Nuclear Technology*, Vol. 92, October issue, pp. 11-29.
- Sen, S., Bergman, W., Hahn, M., and Stormo, J. (2010) On the qualification testing of HEPA filters, Proceedings of the 31st Nuclear Air Cleaning Conference, Charlotte, NC, July 19-21, 2010 www.isnatt.org

Waggoner, C. (2012a) "Is a filter loading qualification test needed?" Proceedings of the 32nd Nuclear Air Cleaning Conference, Denver, CO, June 17-19, 2012

Waggoner, C. (2012b) Personal communication.

Waggoner, C. (2016) Personal communication.

Young, W. C. and R.G. Budynas (2002) Roark's Formulas for Stress and Strain, Seventh Edition, page 502, McGraw-Hill, New York,
materiales.azc.uam.mx/gjl/Clases/MA10_I/Roark%27s%20formulas%20for%20stress%20and%20strain.pdf (copy to web browser, do not click on url)